Titre: Title:	Development, Physics, Technology and Operation of a "Pilot-Scale" Dielectric Barrier Discharge Reactor
Auteur: Author:	Sean Watson
Date:	2019
Type:	Mémoire ou thèse / Dissertation or Thesis
Référence: Citation:	Watson, S. (2019). Development, Physics, Technology and Operation of a "Pilot-Scale" Dielectric Barrier Discharge Reactor [Mémoire de maîtrise, Polytechnique Montréal]. PolyPublie. https://publications.polymtl.ca/4018/

POLYTECHNIQUE MONTRÉAL

affiliée à l'Université de Montréal

Development, Physics, Technology and Operation of a "Pilot-Scale" Dielectric Barrier Discharge Reactor

SEAN WATSON

Département de génie Physique

Mémoire présenté en vue de l'obtention du diplôme de *Maîtrise ès sciences appliquées*

Génie physique

Août 2019

POLYTECHNIQUE MONTRÉAL

affiliée à l'Université de Montréal

Ce mémoire intitulé :

Development, Physics, Technology and Operation of a "Pilot-Scale" Dielectric Barrier Discharge Reactor

présenté par **Sean WATSON**

en vue de l'obtention du diplôme de *Maîtrise ès sciences appliquées*

a été dûment accepté par le jury d'examen constitué de :

David MÉNARD, président
Michael WERTHEIMER, membre et directeur de recherche
Pierre-Luc GIRARD-LAURIAULT, membre

ACKNOWLEDGEMENTS

I would like to express my deep gratitude to Professor Michael R. Wertheimer, my research supervisor, for his patient guidance, and useful critiques of this research work. I would also like to thank Dr. Bernard Nisol, for his counsel and enthusiastic encouragement. Assistance provided by Mr. Yves Leblanc, our lab technician, was also of great support to this work. Finally, I would also like to extend my special thanks to the co-authors of the journal articles presented in this thesis, namely Professor Frédéric Sirois and Professor Sophie Lerouge, Dr. Hervé Gagnon and Mylène Archambault-Caron.

RÉSUMÉ

Ce mémoire fait suite aux recherches précédentes à Polytechnique Montréal dans le domaine des plasmas froids générés dans des décharges à barrières diélectriques (DBD), travail qui continue depuis les années 1980. Ce sujet a été à l'origine de plusieurs mémoires et thèses qui, bien évidemment, ont fait l'objet de nombreux articles publiés dans des revues internationales. Le présent candidat à la maîtrise a fait ses débuts au sein du groupe de recherche en 2015, avant de commencer son programme de M.Sc.A.. Il a été co-auteur de plusieurs articles, dont un exemple est présenté en annexe. Le contenu de ce document, présentant le véritable travail accompli au cours du programme de M.Sc.A., est essentiellement composé autour de 2 chapitres principaux (chapitres 4 et 5) : il s'agit d'articles (le premier déjà publié, le second étant soumis en juin 2019) dont le candidat est l'auteur principal.

Dans le premier article, présenté au chapitre 4, deux réacteurs à DBD de tailles différentes, un petit et l'autre plus grand d'un ratio de ca. 1 : 40, avec leurs équipements associés ainsi qu'un programme Matlab® dédié, ont été utilisés pour déterminer avec précision l'énergie électrique, E_g, dissipée par cycle de la tension (en courant alternatif) appliquée, V_a. Pour le petit réacteur, le tout a été accompli sur une gamme de fréquences entre $5 \leq f \leq 50$ kHz et en utilisant une paire identique de différents matériaux diélectriques (des disques de 2.54 cm de diamètre) possédant une permittivité relative variant entre $2.1 \leq \kappa'_{die} \leq 9.5$, et agissant à titre de barrières diélectriques au sein d'une DBD pour 4 gaz différents : He, Ne, Ar et N_2. Pour le plus grand réacteur, f a été limitée à 20 kHz, et ce dans l'Ar et l'He. Ce dernier système a pour principale utilisation des expériences de polymérisation par plasma, où des « monomères » organiques sont mélangés au flux du gaz porteur : l'Ar. La méthode pour évaluer E_g avec exactitude est d'abord présentée, pour suivre avec une comparaison des valeurs mesurées sous différentes conditions. Dans la mesure du possible, ces valeurs sont comparées entre le petit et le grand réacteur, puis dans un second temps avec les valeurs retrouvées dans la littérature. La fiabilité de la méthode est confirmée, par exemple, du fait de la concordance avec les valeurs de champs de rupture électrique pour les gaz étudiés reprises dans la littérature, de même qu'avec plusieurs autres nouveaux résultats.

Le deuxième article, présenté au chapitre 5, traite de la méthodologie précédemment développée pour comprendre les échanges d'énergie entre les molécules-précurseurs et le gaz porteur d'Ar au sein du grand (à l'échelle pilote) réacteur DBD. L'accent est mis sur une famille de précurseurs organiques simples, c'est-à-dire cinq hydrofluorométhanes, CH_xF_y ($0 \leq x \leq 4$; $y = 4 - x$). Chacun de ces précurseurs (à des concentrations de ‰) a été mélangé avec 10 litres standards par minute (slm) d'Ar dans une DBD à 20 kHz, 8 kV (crête-à-crête). Pour chaque composé, l'énergie absorbée par molécule, E_m a été tracée en fonction des flux de précurseur, F_d (en sccm). Outre la détermination de E_m à partir des mesures électriques telles que mises en place lors de travaux précédents, nous avons étudié la physico-chimie du plasma à l'aide d'une technique de diagnostic supplémentaire, la spectrométrie d'émission optique. L'influence de la structure chimique des précurseurs a été mise en évidence lors de l'étude des dépôts de couches minces de polymères par plasma (PP). De plus, les vitesses de dépôt et les angles de contact de ces films de PP ont été mesurés et corrélés avec les valeurs de E_m et les compositions chimiques déterminées par XPS.

ABSTRACT

This thesis extends earlier research at Polytechnique Montreal in the area of dielectric barrier discharge (DBD) "cold" plasmas, work that commenced as far back as the 1980s; it has over the years been the object of numerous M.Sc.A. / Ph.D. theses and, of course, many articles published in international journals. The present master's candidate started collaborating with the DBD team in 2015, before commencing his own M.Sc.A. program, and has been co-author of several published articles, for example the one presented in the Appendix. The content of this current document, truly the research associated with this M.Sc.A. program, is to a large extent concentrated in two main chapters (Nos. 4 and 5), articles for both of which the candidate is the lead author.

In the first article, Chapter 4, two DBD reactors, one small, the other about 40 times larger, associated equipment and a dedicated Matlab® code have been used to carry out precise determinations of electrical energy, E_g, dissipated per discharge cycle of the applied a.c. voltage, V_a. In the smaller reactor, this was done over the frequency range $5 \leq f \leq 50$ kHz and using twin pairs of several different insulating materials (2.54 cm diameter discs) with relative permittivities between $2.1 \leq \kappa'_{die} \leq 9.5$ as dielectric barriers in DBDs for 4 different gases: He, Ne, Ar and N_2. In the large reactor, f was restricted to 20 kHz in Ar and He; this latter system primarily serves for plasma polymerization experiments in which organic "monomers" are admixed with the flow of Ar as carrier gas. We report the method for exactly evaluating E_g, then present and compare values measured under different conditions. To the extent possible, these are compared between the small and large reactors, and with results published in the literature. The reliability of the method is confirmed, for example, by reproducing published breakdown fields of the gases examined, and by several other original results.

The second article, Chapter 5, deals with this method that we have developed for understanding energetic exchanges between precursor molecules and Ar carrier gas in the large (pilot-scale) DBD reactor. It focuses on a particular family of quite simple organic precursor gases, namely five hydrofluoromethanes, CH_xF_y ($0 \leq x \leq 4$; $y = 4 - x$). Each of those precursors (at ‰ concentrations) was mixed with 10 slm of Ar in a 20 kHz, 8 kV (peak-to-peak) DBD. For each compound, E_m, the energy absorbed per molecule, was plotted as a function of precursor

flow rate, F_{d} (in sccm). Beside determination of E_{m} from electrical measurements of the types perfected in preceding work, we have used optical emission spectroscopy (OES) as a diagnostic of the plasma physico-chemistry. The influence of the precursors' chemical structures has been investigated by depositing thin plasma polymer (PP) coatings; we have measured the deposition rates and water contact angles of these PP films, and have correlated them with E_{m} values and chemical compositions determined from XPS measurements.

TABLE OF CONTENTS

LIST OF TABLES

LIST OF FIGURES

LIST OF SYMBOLS AND ABBREVIATIONS

This list presents the symbols and abbreviations used in the thesis in alphabetical order, along with their meanings.

A	Area
a.c.	Alternating Current
a.f.	Audio Frequency
AP	Atmospheric Pressure
APGD	Atmospheric Pressure Glow Discharge
APTD	Atmospheric Pressure Townsend Discharge
C_1	Parasitic Capacitance (c.f. Fig 4.2)
C_2	Parasitic Capacitance (c.f. Fig 4.2)
CAG	Contact Angle Goniometry
C_{die}	Capacitance of the Dielectric (c.f.Fig 4.2)
C_{gap}	Calculated Gap Capacitance (c.f. Fig 4.2)
d	Dielectric Thickness (c.f. Eq. 4.2)
DBD	Dielectric Barrier Discharge
E_{a}	Activation Energy
ΔE_{g}	Energy Difference (pure - mixture)
E_{g}	Electrical Energy Input
E_{m}	Energy per Molecule
F	Carrier Gas Flow (mainly Ar)
f	Frequency
F_{d}	Precursor-Molecule Flow
FWHM	Full Width at Half Maximum
G	Reactor- and Process Dependant Factor
HV	High Voltage
I	Current
I_{d}	Discharge Current (c.f. Fig 4.2)
I_{g}	Gas Current (c.f. Fig 4.2)
I_{gap}	Gap Current (c.f. Fig 4.2)
I_{m}	Measured Current (c.f. Fig 4.2)
ITO	Indium-Tin-Oxide
J_{m}	Emission Intensity per Molecule
κ'	Relative Permittivity
LP	Low Pressure
M	Molecular Mass
n	Number of Cycles
OES	Optical Emission Spectroscopy
P	Power
PP	Plasma Polymer
PECVD	Plasma Enhanced Chemical Vapor Deposition
PTFE	Poly(tetrafluoroethylene)
Q	Charge
r	Deposition Rate
r.f.	Radio Frequency
r_{m}	Mass Deposition Rate per Unit of Monomer Flow
R_{m}	Precision Resistance = 50 Ω (c.f. Fig 4.2)
sccm	Standard cm^3/minute
slm	Standard L/minute
T	Kinetic Temperature

V	Potential Difference
v	Volume
V_{a}	Cell Potential (c.f. Fig 4.2)
V_{die}	Potential across C_{die} (c.f. Fig 4.2)
V_{gap}	Gap Potential (c.f. Fig 4.2)
V_{m}	Measured Potential across R_{m} (c.f. Fig 4.2)
V_{ps}	Source Potential (c.f. Fig 4.2)
W	Power Input
WCA	Water Contact Angle
XPS	X-Ray Photoelectron Spectroscopy
‰	Parts per Thousand
Z_{d}	Discharge Impedance (c.f. Fig 4.2)

LIST OF APPENDICES

CHAPTER 1 INTRODUCTION

A plasma is a partially- or fully-ionised gas. It can be generated at low pressure (LP, partial vacuum, typically near 1 millibar or 100 Pa) or at atmospheric pressure (AP, 100 kPa). Figure 1.1 shows (a) a LP plasma between two electrodes in a glass reactor; (b) an AP plasma "jet"; (c) a so-called dielectric barrier discharge (DBD) plasma, the type that will exclusively be discussed hereafter in this thesis. A DBD plasma is formed by applying a high alternating-current (ac) voltage in the gap between two electrode surfaces, at least one of which is covered by a dielectric. Further information on the topic of DBD will be presented and discussed in Chapter 2. All plasmas shown in (a), (b) and (c) are "cold", that is, the gas temperature remains close to 300 K.

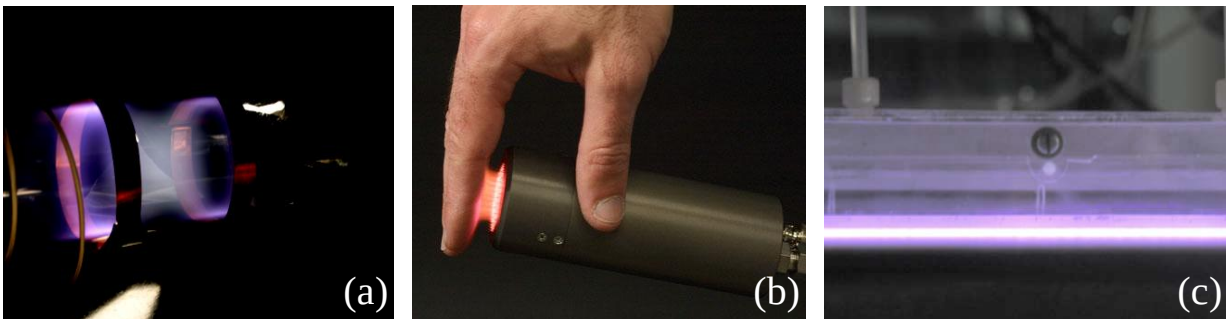

Figure 1.1. DBD reactors used in 3 different applications: (a) low-pressure system, reprinted with permission from [1], (b) atmospheric pressure plasma torch configuration (© Surfx Technologies LLC, used with permission), (c) atmospheric pressure planar DBD configuration, reprinted with permission from [2].

Over the course of many years, beginning in the 1980s, Prof. Wertheimer's laboratory at Polytechnique Montréal has been conducting experimental research involving DBD, high-voltage (HV) breakdown of gases at AP, first at power frequency (60 Hz) in air or its constituents [3, 4], but more recently at audio-frequency (typically 20 kHz) in noble gases such as He [5-7]. The objectives of those studies were, first, to investigate the physico-chemical degradation of polymers that played the role of dielectric barriers [3, 4], later to characterize the "atmospheric pressure glow discharge" (APGD) behavior of He first reported in 1969 by R. Bartnikas [5].

Those early studies then morphed into yet others [8, 9] that laid the important groundwork for research presented in this M.Sc.A. thesis, namely the development of a precise method for measuring electrical energy input, E_g, primarily into He APGD; combined with accurate

temperature (T) measurements, this enabled one to perform a detailed calorimetric (heat balance) investigation. A key objective of research presented in this thesis has been to further investigate and exploit the precise methods for measuring E_g into all noble gas DBD plasmas with the aid of two home-built DBD reactors with very different characteristics [8, 9]. Accurate knowledge of E_g is important for several reasons: (i) in the case of pure noble gas discharges, it helps confirm that one has good, reliable understanding of the plasma physics involved; (ii) more important, as will be shown later, E_g measurements have opened the way to measure energy uptake by molecular "dopant" gases that are added in very small (typically parts-per-thousand, ‰) concentrations to the noble carrier gas flow (see below). Surprisingly, little published work of this type can be found in the literature, but all is based on modeling of the plasma discharges, also addressed in later sections. The earliest reported E_g values in He atmospheric pressure (AP) DBD were those of Decomps et al. [10], followed later by power density measurements of Nersisyan and Graham [11], while Hofmann and coworkers reported power dissipation in AP He and Ar radio-frequency (r.f.) plasma jets [12]. Values of E_g in uniform AP DBD in Ar were discussed by Tyata et al. [13], while Merbahi et al. [14] reported E_g for mono-filamentary Ar micro-discharges.

Another paper from this laboratory [9] reported how E_g, now measured in Ar DBD, could lead to E_m, the average energy absorbed per molecule of a "dopant" gas or vapor from the Ar plasma "energy reservoir", the dopant being introduced at ‰ concentration into the Ar carrier gas flow. This powerful new methodology subsequently gave rise to an extensive series of studies wherein organic precursor (or "monomer") molecular dopants led to deposition of thin plasma polymer (PP) film coatings [9, 15-17]. The author of this thesis has participated very actively in most of that research, even as principal author in certain parts thereof, for example the second article (Chapter 5) in this thesis. However, he also first conducted a comparative study of the two technologically important noble gases, He and Ar, in their pure state, using two DBD reactor systems ("small", area A = 5.1 cm^2; and "large", area A = 216 cm^2), the first article (Chapter 4) in this thesis.

The objectives of this M.Sc.A. thesis can therefore be described as follows:

(a) To help extend the traditional strengths in DBD research that this laboratory has developed over the course of many years. An important task will be to thoroughly assess transferability of

the energy measurement methodology using two very distinct home-built DBD reactors fed with either Ar or He;

(b) More particularly, to further exploit the powerful methodology for precise energy measurements in (pure or "doped") noble gas DBD plasmas [8, 9, 15]. We will here focus on the effect of electronegative atoms (such as F) in dopants on (1) the physico-chemical composition and the homogeneity of discharges, and (2) the validity of our energy measurement methodology in potentially difficult cases like filamentary, CF_4-doped Ar discharges.

(c) In an even more general way, another sub-objective can be stated as follows: "Cold" DBD plasmas are of very great scientific and technological interest, wherein the latter extends over many diverse fields including (i) ozone generation; (ii) ultraviolet light sources; (iii) surface modification of polymers for adhesion enhancement; (iv) plasma-enhanced chemical vapor deposition (PECVD) of thin coatings; and more recently (v) plasma medicine, a very rapidly expanding multi-disciplinary topic involving not only physicists and chemists, but also biologists and clinicians. The review article by U. Kogelschatz [18] gives an even more complete list of applications, but also the underlying fundamental science: even though that paper is now 16 years old, it remains one of the most-cited references and introductions for newcomers to this field. Therefore, another sub-objective here is to *help advance fundamental and practical aspects of DBD plasma science*.

To help understand how these objectives connect with this AP plasma research, a short state-of-the-art review will first be offered in Chapter 2, and an overview of the document's organization in Chapter 3. From there, the thesis will expand by presenting two relevant research articles, the first (Chapter 4) pertaining to electrical measurements of the AP plasma discharge in noble gases; the second (Chapter 5) shows how this particular methodology is used to analyze PP deposition (AP-PECVD) in the specific case of hydrofluoromethanes. A presentation of the findings with respect to the electrical characterization of plasma will follow, before discussing further research objectives and possible improvements to the current methodology which might be explored.

We now continue, in Chapter 2, to present an overview of the literature that has been most relevant to the context of this thesis.

CHAPTER 2 CRITICAL LITERATURE REVIEW

2.1 General Considerations

DBD for plasma processing at AP have been gaining importance, to a large extent because they obviate the need for costly vacuum systems. In his review article, Kogelschatz described in detail the physics of this thermodynamically non-equilibrium (*cold*) plasma, along with its uses in numerous plasma-chemical reactions such as ozone synthesis, surface modification of polymers, abatement of pollutants, and excimer lamps [18]. Indeed, many gases, but especially the noble gases, can serve as efficient emitters of ultraviolet (UV) and vacuum-UV (VUV) radiation [18-22].

Generally, AP DBDs under audio-frequency (ca. 10 kHz and up) alternating current (a.c.) conditions are filamentary, comprising many ultra-rapid constricted micro-channels (streamers) that occur pseudo-randomly over the dielectric surface, a charge transfer occurring at each discharge site on the electrodes [18]. However, in 1969, Bartnikas [5] reported that a.c. discharges in He can manifest glow that extends uniformly over the entire electrode surface [6, 10, 23, 24]. Now often termed *atmospheric pressure glow discharges* (APGDs) on account of their spatially homogenous appearance, they have also been reported in other gases and gas mixtures [25, 26]. Figure 2.1(a) illustrates filamentary (streamer) discharge in air, while (b) shows the uniform "glow" (APGD) discharge that covers the entire surface area of the electrodes. In both cases, the images were acquired perpendicularly through a transparent indium-tin-oxide (ITO)-coated glass plate, ITO serving as the conducting ground electrode.

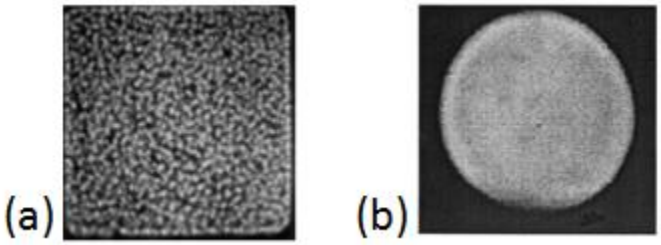

Figure 2.1. (a) Filamentary discharges in air at 1 bar; (b) dielectric barrier APGD in a flow of pure He at 1 bar (Reproduced with permission from [27]).

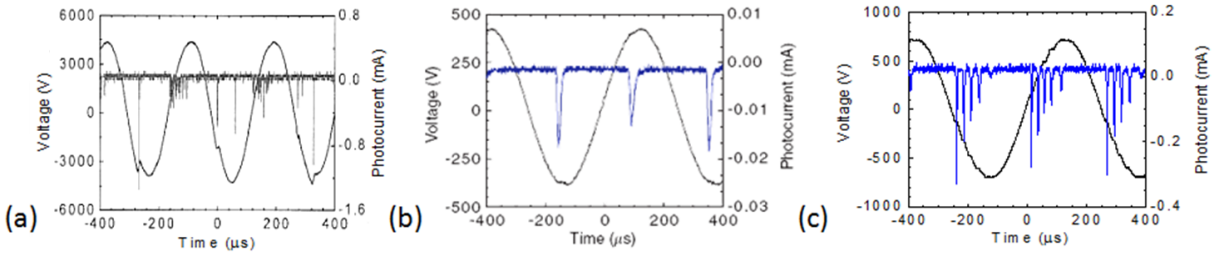

Figure 2.2. (a) Filamentary (streamer-) discharges in an air gap at 4 kV peak voltage; (b, c) *Pseudo-glow* behavior at 2 kHz in a 0.5-mm helium gap under atmospheric pressure, with peak voltage across the metallic-dielectric electrode gap as a parameter. (b) 430-V peak (c) 720-V peak. (Reproduced with permission from [7]).

Figure 2.2(a,b,c) shows (sinusoidal) voltage and superimposed current oscillograms, where (a) corresponds to Figure 2.1(a), and (b,c) to Figure 2.1(b). Regarding (a), the multitudes of streamer discharges in air or O_2, generally in electronegative gases, are characterized by very short (a few ns) duration current pulses and small (ca. 100 μm) diameters that give rise to the luminous spot-footprints in Figure 2.1(a). But in this present work we shall be dealing further with the filamentary type of discharges only sporadically (Figure 2.1(a) and Figure 2.2(a)), rather with the "glow-type" (APGD) discharges of the types illustrated in Figure 2.1 (b) and Figure 2.2 (b,c); more will be said about these further below.

Apart from Kogelschatz [18], Massines and coworkers also published more recent comprehensive reviews of APGD physics, including their own seminal contributions [25, 26]. For example, it is known that Penning transfer via energetic metastables (He*, 19.8 eV lowest energy level; and Ne* (Neon), 16.6 eV) or dimers (He_2, Ne_2) can efficiently ionize residual traces of atmospheric or other gaseous impurities, giving rise to a so-called *memory effect* and a lowering of the breakdown voltage [25, 26]. For these reasons, they are also referred to as *Penning mixture*. Pure nitrogen (N_2) is another gas in which APGD-like behavior can be observed [6, 28]. However, as explained by Massines and coworkers [25, 26, 28], its discharge physics is quite distinct and this has led them to coin for it the term APTD (Townsend) discharge.

APGD in He and Ne is characterized by a short-duration (ca. 5 μs) current peak per half cycle of the applied a.c. voltage, see Fig. 2(b), while the current peak is of much longer (tens of

μs) duration for APTD [6, 25, 26, 28]. However, a noteworthy feature of He and Ne APGD is the possible appearance of one or more additional current peak(s) per half-cycle under certain conditions, namely when the applied voltage is sufficiently high, and/or with deliberate addition of a gaseous dopant, see Fig. 2(c); this has been termed *pseudo-glow* by Bartnikas et al. [5-7]. Therefore, to distinguish the two situations, we shall hereafter refer to them as *single peak* (Fig. 2(b)) and *multi-peak* (Fig. 2(c)) regimes, respectively. Other key characteristics of APGD and APTD are the virtually perfect reproducibility, over very long durations, of the multi-μs current peaks' time-span and amplitudes [5-7, 10, 23, 24, 26, 28, 29]. It is this latter feature that enables measurements of the type reported in this present work.

In recent years, AP DBDs have also gained prominence for the deposition of thin films [2, 25, 30] (see section 2.2. below) and in so-called "plasma medicine" [31]. In most of those applications, it is essential that the gas (kinetic) temperature, T, remain near ambient, slightly above 300 K. This laboratory has shown that reliable T measurements are best carried out by using fiber-optic thermometers [8, 32]; commercial fiber-optic thermometers were developed for use in conditions involving high voltages and/or intense electromagnetic fields, where conventional (e.g. thermocouple) instrumentation must be disqualified. The use of fiber-optic thermometers, however, is surprisingly not a widespread practice even though it was clearly shown that determination of T based on optical emission spectroscopic (OES) techniques invariably overestimates the true gas temperature, often very grossly [32, 33].

Beside measuring T, it is clearly important for the operator of a (AP) plasma system to also know the exact amount of electrical power, P, delivered to the plasma and hence also to a substrate. Now, in many low-pressure (LP) plasma systems (r.f., or microwave), electrical power measurements can be carried out relatively accurately, albeit with some pitfalls and sources of uncertainty. But there is good reason to believe that, for power measurements in AP DBD plasmas, this is not the case. For example, many researchers use *Q-V plots*, also known as Lissajous figures [13, 34-36]; first introduced by Manley in 1943 [35, 37], this technique is now known to require considerable caution.

Chapter 4 of this thesis is devoted to exploiting the methodology developed in this laboratory for measuring power (or, rather E_g, the energy per cycle of the applied audio-frequency voltage)

[9] to a comparative study of two noble gases, He and Ar, in two very different DBD reactor systems.

2.2 DBDs for Use in PECVD

The literature regarding deposition of thin organic films for practical uses by plasma-enhanced chemical vapor deposition (PECVD), also known as plasma polymerization (PP), goes back at least to the early 1960s [38]. During subsequent decades, thousands of articles devoted to this subject have been published worldwide, as well as several monographs [39, 40]. While earlier literature almost exclusively dealt with high-frequency, r.f., or microwave glow-discharge plasmas sustained at reduced pressure, typically near 100 mTorr (13.3 Pa), there has more recently been growing interest in PP based on atmospheric pressure AP plasmas [25, 36, 41-47]. DBD constitute the main approach that enables scale-up for industrial processing, because they obviate the need for vacuum systems and can thereby potentially reduce costs significantly, as already pointed out in section 2.1. above.

In the PP literature, there has long been an interest in correlating deposition kinetics, physico-chemical and structural properties of films with energy absorbed by the organic precursor (*monomer*) molecules in the plasma. Indeed, this often controversial subject has been the object of a series of *debates* in the journal *Plasma Processes and Polymers* [48]: Hegemann and coworkers [49-51] developed an original approach towards the macroscopic phenomenology of PP, one which leads to an unifying dependence of the mass deposition rate per unit of monomer flow, r_m/F, on the macroscopic reaction parameter W/F (W here being power input), by way of a quasi-Arrhenius expression:

$$r_\mathrm{m}/F \;=\; G\, exp[-E_\mathrm{a}/(W/F)] \tag{2.1}$$

where E_a is an apparent activation energy, and G a reactor- and process-dependent factor related to the maximum monomer conversion into film growth. W/F, proportional to the average energy transferred per monomer molecule during its travel through the active plasma zone, governs the formation of reactive intermediates. It was originally known as the Becker parameter [52], or since the late 1970s as the Yasuda parameter [39, 53], W/FM (energy per mass of monomer), M being molecular mass of the monomer. The use of Eq. (2.1) in plots of r/F versus W/F allows one to

identify different regimes in the PP process, for example “monomer-rich” and “monomer-lean” ones; these usually lead to films with significantly differing structures and characteristics. An important motivation of Hegemann’s work has been to develop their macroscopic approach to facilitate reactor scale-up, and to permit comparison of data from different laboratories.

Implementation of the concepts just described is relatively straightforward in the case of high frequency (h.f.) low pressure (LP) PP, for the following reasons; (i) usually, the monomer is introduced into the plasma reactor undiluted, although Hegemann and coworkers have shown how their method can be used also for mixtures including a second (reactive, but non-polymerizing) gas [49, 50]; (ii) while not simple and unambiguous, it is often possible to measure power absorbed in h.f. plasmas with reasonable precision. Now, in the case of AP discharges, particularly for PP reactions, neither of these generally apply:

(i) First, AP PP processes necessarily use a flow of (inert) carrier gas wherein that of the monomer is generally highly diluted (typically in the ‰ range);

(ii) regarding power measurements in AP plasmas, we have every reason to believe (see section 2.1. above) that such measurements are far from being simple, certainly not those involving AP DBDs.

Although various authors have proposed and attempted to use the Yasuda parameter in the context of AP DBD PP [36, 45-47, 54], combined complications (i) and (ii) above have so far presented major obstacles. Now, the precise method for measuring E_g, the energy dissipated per cycle of the applied a.c. voltage in noble gas AP DBD developed in this laboratory [8, 55], results in reliable data, based on objective assessment criteria discussed elsewhere [8] and later in this thesis (Chapter 4). Referring to objective (b) in Chapter 1, an important sub-objective has been to further investigate whether E_g measurements can yield specific information about PP reactions when a small precursor addition in 10 slm of Ar carrier constitutes only a few ‰ (or less) of total feed gas flow into the DBD reaction zone; the particular precursor family examined here has been the family of five hydrofluoromethanes (CH_xF_y, ($0 \leq x \leq 4$; $y = 4 - x$); PECVD of AP DBD reactions in this family of compounds constitutes the entirely novel content of Chapter 5.

CHAPTER 3 ORGANIZATION OF THE DOCUMENT AND COHERENCE OF THE ARTICLES IN RELATION TO THE RESEARCH GOALS

3.1 Introduction

Chapters 1 (***Introduction***) and 2 (***Critical Literature Review***) have presented the concepts, context, background and earlier work (both in this laboratory and elsewhere) underlying the research described in this M.Sc.A. thesis.

Chapters 4 and 5 provide two articles, both already published in international journals with peer review systems; their titles are

(i) "**Energetics of noble gas dielectric barrier discharges (DBD): Novel results related to electrode areas and dielectric materials**";

(ii) "**Energetics of reactions in a dielectric barrier discharge with argon carrier gas: viii hydrofluoromethanes**".

Those two articles are presented integrally, the only major modification being that all references have been combined in numerical order with the preceding lists from Chapters 1 and 2 in the overall summary bibliography at the end of this document. Both articles are complete documents, ones that contain practically all the information required for the reader to fully understand the content. Now, this requirement must, of course, also apply to this thesis, a document of more elaborate content than the two articles and its preceding chapters. Another important piece of information from earlier work in this laboratory [9] is therefore provided in the sub-section to follow. It will act as the "glue" between Chapters 4 and 5, so to speak. To avoid excessive repetition, we shall be referring to symbols and methods presented in those chapters whenever called for, for example in section 5.2, (Experimental) of Chapter 5. For further assistance with the symbols, the reader is kindly referred to the list of symbols and abbreviations presented at p. xiv-xv.

3.2 Evaluation of E_m from ΔE_g

An earlier article from this laboratory [9] described the method by which one evaluates the key parameter E_m (in eV), the energy per precursor molecule that is central to the content of Chapter 5. It was derived from the energy difference, ΔE_g, associated with the precursor admixture to the 10 slm pure Ar carrier gas flow under the very same other experimental conditions (reactor geometry, applied high voltage (HV) frequency, amplitude, etc.). Chapter 4 presents the equivalent circuit model and MATLAB® program used to determine E_g (in μJ), the energy dissipated in the pure AP DBD plasma during each applied a.c. HV cycle. An important required piece of information is therefore to present the intervening steps between E_g, ΔE_g, and E_m.

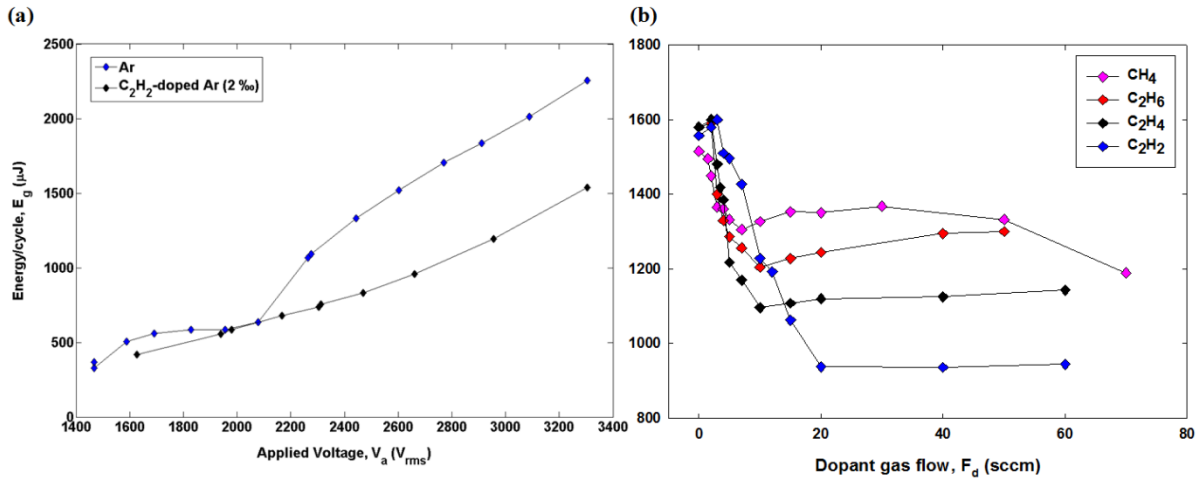

Figure 3.1. (a) Comparison of E_g versus V_a (rms) between pure Ar (F = 10 slm, upper curve) and acetylene-doped Ar (F_d = 20 sccm, lower curve) DBD plasmas at 20 kHz. (b) Plots of E_g versus precursor gas flow, F_d, for Ar (F = 10 slm) DBD plasmas "doped" with hydrocarbons. The frequency was f = 20 kHz and the applied voltage, V_a = 2.8 kV_{rms}. Reproduced with permission from [9].

Figure 3.1. (a) shows the curves for 20 kHz DBD plasmas, the upper and lower ones respectively corresponding to the pure Ar carrier gas (10 slm), and with addition of 20 sccm (2 ‰) of acetylene (C_2H_2). For V_a > 2400 V_{rms}; ΔE_g is seen to remain near-constant between the upper (*pure*) and lower, precursor loaded, branches. The next step was then to measure ΔE_g using

fixed parameters for V_a = 2.8 kV_{rms}, and f = 20 kHz, while changing the concentration of the added reagent ("dopant") gas flow, F_d. This exercise was carried out not only for C_2H_2, but also for other hydrocarbons (CH_4, C_2H_6, C_2H_4), resulting in the measurements shown in Figure 3.1. (b).

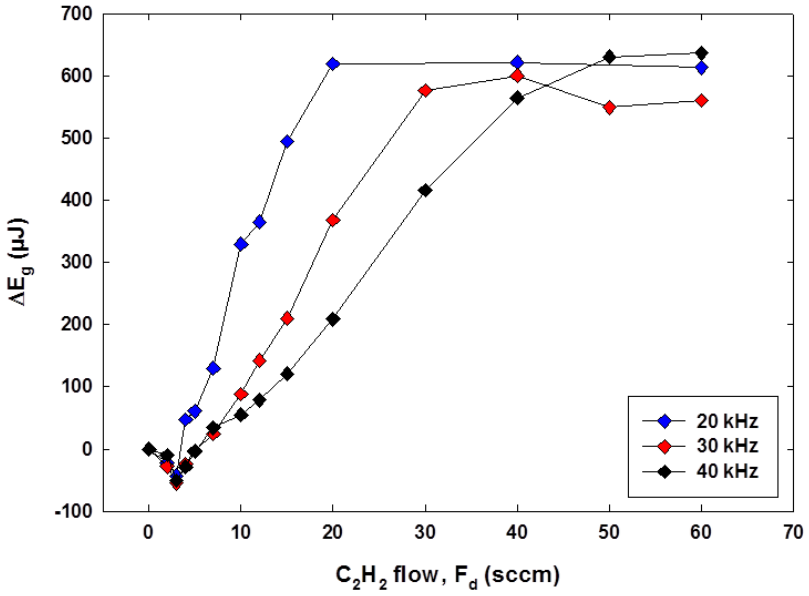

Figure 3.2. Plots of absorbed energy difference, ΔE_g, versus C_2H_2 flow, F_d, for Ar (F = 10 slm) DBD plasmas at 20, 30 and 40 kHz. The applied voltage, V_a, was 2.8 kV_{rms}. Reproduced with permission from [9].

The first, tentative, interpretation for the different hydrocarbon curves implied identifying the two regimes. For $F_d < (F_d)_{crit}$, a certain "critical" precursor flow rate, all molecules and most of their fragments undergo reaction during their residence time in the plasma zone, a condition that will be further addressed as the *monomer-lean regime*. For $F_d > (F_d)_{crit}$, a certain fraction may escape without reacting (completely), or by consuming energy via a different set of channels, hence resulting in a *monomer-rich regime*. To test this hypothetical interpretation, we now plot (Figure 3.2) values of ΔE_g, the energy difference (per cycle) between the case of pure Ar [~1600 μJ, see Figure 3.1.(a)] and Ar with a flow, F_d, of C_2H_2 additive, versus F_d, corresponding to f = 20, 30 and 40 kHz. We calculate the energy consumed per molecule under the presumed condition where *all* C_2H_2 molecules *just* appear to have been converted in the plasma, namely at

the very beginning of the plateau regions in Figure 3.2, corresponding to $(F_{\mathrm{d}})_{\mathrm{crit}}$. For the case of 20 kHz, and during a one-second time interval, the total energy absorbed by the C_2H_2 molecules, E_{tot}, is:

$$E_{\mathrm{tot}} = \Delta E_{\mathrm{g}} \times f \cong 600\ \frac{\mu\mathrm{J}}{\mathrm{cycle}} \times 20 \times 10^3\ \mathrm{cycles}$$

$$E_{\mathrm{tot}} = 12\ \mathrm{J} \times 6.24\ \times 10^{18}\ \frac{\mathrm{eV}}{\mathrm{J}} = 7.49\ \times 10^{19}\ \mathrm{eV} \tag{3.1}$$

Figure 3.2. shows that the plateau is reached at $(F_{\mathrm{d}})_{\mathrm{crit}}$ = 20 sccm; the corresponding number of molecules, N, entering into the discharge zone is, at 295 K:

$$N = 20 \times 10^{-3}\ \frac{\mathrm{L}}{\mathrm{min}} \times \frac{1}{24}\ \frac{\mathrm{mol}}{\mathrm{L}} \times 6.022 \times 10^{23}\ \frac{\mathrm{molec}}{\mathrm{mol}} = 5 \times 10^{20}\ \frac{\mathrm{molec}}{\mathrm{min}},$$

or, for the one-second time interval:

$$N = \ 8.3 \times 10^{18}\ \frac{\mathrm{molec}}{\mathrm{s}} \tag{3.2}$$

Therefore, energy consumed per molecule is, from (3.1) and (3.2):

$$\frac{E_{\mathrm{tot}}}{N} = 7.49\ \times 10^{19} / 8.3 \times 10^{18} = 9.0\ \frac{\mathrm{eV}}{\mathrm{molec}} \tag{3.3}$$

From Figure 3.2., we note that for f = 30 and 40 kHz, $(F_{\mathrm{d}})_{\mathrm{crit}}$ ~ 30 and ~ 40 sccm, respectively; therefore, the value $\frac{E_{\mathrm{tot}}}{N}$ = 9.0 $\frac{\mathrm{eV}}{\mathrm{molec}}$ remained constant for all three conditions. This tends to confirm the *total conversion* hypothesis proposed above. Considering that C≡C (~8.7 eV) bond-breakage occurs very close to the above-calculated value of 9 eV, it can be concluded that the methodology for evaluating E_{m} (= $\frac{E_{\mathrm{tot}}}{N}$) is physically meaningful, a conclusion that subsequently proved reliable in a large variety of contexts (different families of organic molecules, of course including not only the hydrocarbons in Figs. 3.1. and 3.2. above, but also others) [9]. In the Appendix we present further examples of E_{m} evaluations as they pertain to organic acids and other organic precursor compounds.

Having now provided adequate, detailed background information about evaluation of E_{m}, it is possible to advance to presentations of Chapters 4 and 5.

CHAPTER 4 ARTICLE 1: ENERGETICS OF NOBLE GAS DIELECTRIC BARRIER DISCHARGES: NOVEL RESULTS RELATED TO ELECTRODE AREAS AND DIELECTRIC MATERIALS

Sean Watson, Bernard Nisol, Hervé Gagnon, Mylène Archambault-Caron,

Frédéric Sirois, Michael R. Wertheimer.

Article published in:

IEEE Transactions on Plasma Science, Vol. 47, No. 5, pages 2680 – 2688, May 2019

Energetics of Noble Gas Dielectric Barrier Discharges (DBD): Novel Results Related to Electrode Areas and Dielectric Materials

Abstract— Two dielectric barrier discharge (DBD) reactors, one small, the other about 40 times larger, associated equipment and a dedicated Matlab® code have been used to carry out precise determinations of electrical energy, E_g, dissipated per discharge cycle of the applied a.c. voltage, V_a. In the smaller reactor, this was done over the frequency range $5 \leq f \leq 50$ kHz and using twin pairs of several different insulating materials (2.54 cm diameter discs) with relative permittivities between $2.1 \leq \kappa'_{die} \leq 9.5$ as dielectric barriers in DBDs for 4 different gases: He, Ne, Ar and N_2. In the large reactor, f was restricted to 20 kHz in Ar and He; this latter system primarily serves for plasma polymerization experiments in which organic "monomers" are admixed with the flow of Ar as carrier gas. We report the method for exactly evaluating E_g, then present and compare values measured under different conditions. To the extent possible, these are compared between the small and large reactors, and with results published in the literature. The reliability of the method is confirmed, for example, by reproducing published breakdown fields of the gases examined, and by several other original results.

Index Terms— Dielectric barrier discharge (DBD); atmospheric pressure (AP); cold plasma; small and large reactors; permittivity; noble gas; energy dissipation; APGD.

4.1 Introduction

Dielectric barrier discharges (DBD) for plasma processing at atmospheric pressure (AP) have been gaining importance because they obviate the need for costly vacuum systems. As indicated by its name, this discharge type, including AP glow discharges, APGD, may be obtained in gaps between two electrode surfaces where at least one of them is covered by a dielectric. In his well-known review article, Kogelschatz described in detail the physics of this thermodynamically non-equilibrium (*cold*) plasma, along with its uses in numerous plasma-chemical reactions such as ozone synthesis, surface modification of polymers, abatement of pollutants, and excimer lamps [18]. More recently, AP DBDs have also gained prominence for the deposition of thin films [2, 25, 30] and in so-called "plasma medicine" [31]. In most of these applications, it is essential that the gas (kinetic) temperature, *T*, remains near ambient, slightly above 300 K. We have shown that

reliable gas temperature measurements are best carried out by using fiber-optic thermometers [8, 32], but beside measuring *T*, it is clearly important for the operator of an AP plasma system to also know the exact amount of electrical power, *P*, delivered to the plasma and hence also to a substrate. Now, in many LP plasma systems (radio-frequency, r.f., or microwave), electrical power measurements can be carried out relatively accurately, albeit with some pitfalls and sources of uncertainty. But there is good reason to believe that, for power measurements in AP DBD plasmas, this is not the case. For example, many researchers use *Q-V plots*, also known as Lissajous figures [13, 34, 35, 45]. First introduced by Manley in 1943 [35, 37], this technique is now known to require considerable caution [35].

In two earlier articles [8, 9], we laid important groundwork for research that is presented here: in the first, we reported development of a precise method for measuring electrical energy input, E_g, primarily into He APGD; combined with fiber-optic *T* measurements, it enabled us to perform a detailed calorimetric (heat balance) investigation. The second paper, reference [9], showed how E_g, now measured in Ar DBD, could lead to E_m, the average energy absorbed per molecule of a "dopant" gas or vapor from the Ar plasma "energy reservoir", the dopant being introduced at typically ‰ concentration into the Ar carrier gas flow. This powerful new methodology gave rise to a subsequent, still ongoing, series of studies wherein the dopants, organic "monomer" molecules, led to deposition of thin plasma polymer film coatings [9, 15, 16].

Therefore, a key objective of the research presented here has been to further investigate and exploit the precise methods for measuring electrical energy input into noble gas DBD plasmas, E_g, with the aid of the two above-mentioned home-built DBD reactors with very different characteristics [8, 9]. Surprisingly, little published work of this type can be found in the literature, but all is based on electrical modeling of the plasma discharges. The earliest reported "E_g" values in He AP DBD were those of Decomps et al. [10], followed later by power density measurements of Nersisyan and Graham [11] Innovative aspects of the present work are not only to compare our unique E_g measurement technique among reactors of vastly differing sizes in this laboratory, using He and Ar along with different dielectric barrier materials, and then to compare those results with ones reported in the literature, but also to possibly use it as a tool for facilitating

industrial scale-up of DBD technology. The two DBD reactors used here are described in the following section.

4.2 Experimental Methodology

4.2.1 Dielectric Barrier Discharge Reactors

Two DBD plasma reactors, one small (electrode area, A = 5.1 cm^2), the other much larger (A = 216 cm^2) and ancillary systems are respectively depicted in Fig. 4.1 (a) and (b). Both have been separately described in earlier papers [8, 9], so this needs not be repeated here in detail. While the small reactor has mainly served for plasma diagnostics [8], the larger one is used for deposition of organic coatings, so-called plasma polymers, based on mixtures of a noble carrier gas (argon, Ar) and highly diluted admixtures of volatile hydrocarbons [56].

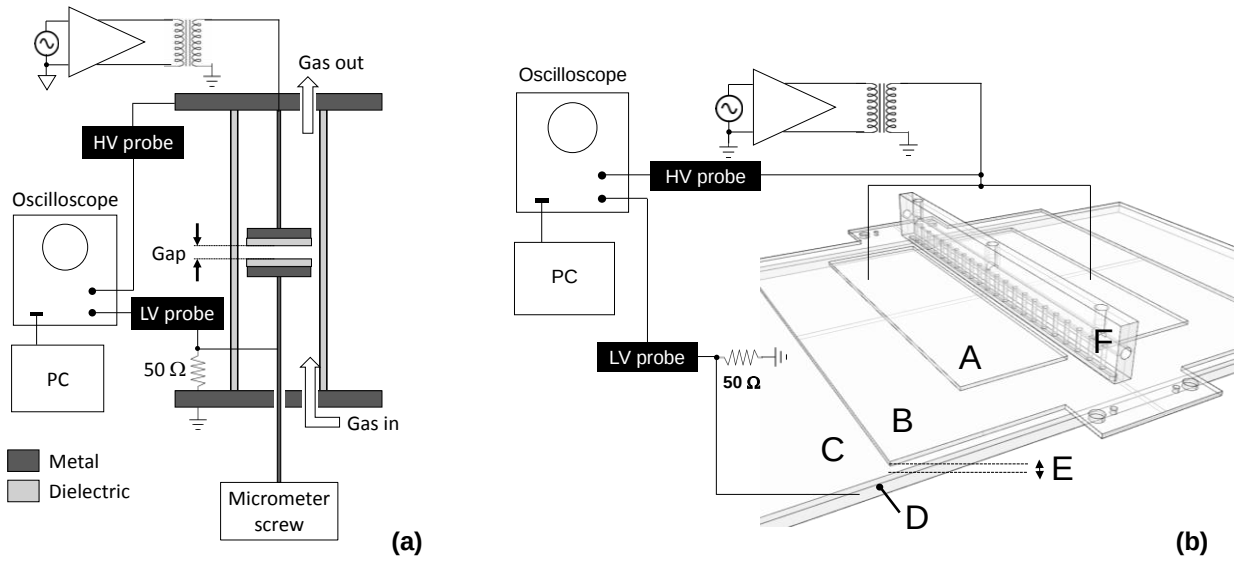

Figure 4.1. (a) Schematic diagram of the small DBD cell and associated components; (b) scale drawing of the large DBD reactor: upper electrodes (**A**); lower electrode (**D**); dielectric barriers (**B, C**); discharge gap (2 mm) (**E**); gas injector / diffuser (**F**).

It is nevertheless important to briefly describe the electrical system: The upper electrodes in (a) and (b) were connected to a HV power supply comprising a variable-frequency a.c. generator (0.5 Hz to > 50 kHz, Hewlett-Packard 3310A), a power amplifier (QSC Ltd., Model RMX2450), an HV transformer (Enercon, Model LM2727-03), and an impedance matching transformer. The

a.c. power supply voltage, $V_{\mathrm{ps}}(t)$, was measured using an HV probe (Tektronix P6015A). For both setups, the lower electrode was connected to ground via a 50 Ω precision resistor, which served to measure the discharge current pulse amplitude and shape.

It is of interest to examine how the energy E stored in the capacitor, C, representing the series combination of both (top and bottom) dielectric barriers and the gap, might affect the value of E_{g}. The charge Q of this capacitor is related to the potential V by the following equation:

$$Q = CV, \text{ where} \tag{4.1}$$

$$C = \frac{\kappa'_{\mathrm{die1}}\kappa'_{\mathrm{die2}}\kappa'_{\mathrm{gap}}\varepsilon_0 A}{\kappa'_{\mathrm{die1}}\kappa'_{\mathrm{die2}}d_{\mathrm{gap}} + \kappa'_{\mathrm{die2}}\kappa'_{\mathrm{gap}}d_{\mathrm{die1}} + \kappa'_{\mathrm{die1}}\kappa'_{\mathrm{gap}}d_{\mathrm{die2}}}. \tag{4.2}$$

In (4.2), ε_0 represents the permittivity of vacuum; $\kappa'$is the relative permittivity; A is the area; d is the thickness and subscripts $\mathrm{die1}$, $\mathrm{die2}$ and gap respectively correspond to the top, bottom and gap (gas) dielectrics. When the top and bottom dielectrics are the same ($\kappa'_{\mathrm{die}} = \kappa'_{\mathrm{die1}} = \kappa'_{\mathrm{die2}}$, and $d_{\mathrm{die}} = d_{\mathrm{die1}} = d_{\mathrm{die2}}$), (2) simplifies to:

$$C = \frac{\kappa'_{\mathrm{die}}\kappa'_{\mathrm{gap}}\varepsilon_0 A}{\kappa'_{\mathrm{die}}d_{\mathrm{gap}} + 2\kappa'_{\mathrm{gap}}d_{\mathrm{die}}}. \tag{4.3}$$

The energy E stored in a capacitor charged up to a potential of V is given by:

$$E = \int_0^V Q dV = \int_0^V CV dV = \frac{CV^2}{2} =$$

$$\frac{1}{2}\left[\frac{\kappa'_{\mathrm{die1}}\kappa'_{\mathrm{die2}}\kappa'_{\mathrm{gap}}\varepsilon_0 A}{\kappa'_{\mathrm{die1}}\kappa'_{\mathrm{die2}}d_{\mathrm{gap}} + \kappa'_{\mathrm{die2}}\kappa'_{\mathrm{gap}}d_{\mathrm{die1}} + \kappa'_{\mathrm{die1}}\kappa'_{\mathrm{gap}}d_{\mathrm{die2}}}\right]V^2. \tag{4.4}$$

Clearly, both κ'_{die} and d_{die} determine E, hence they most likely also affect E_{g}. Accordingly, we have investigated a series of different dielectrics with $2.1 \leq \kappa'_{\mathrm{die}} \leq 9.5$ but constant thicknesses, $d_{\mathrm{die}} = 2$ mm (see Table 4.1). The method for evaluating the electrical energy dissipated in the gas discharge per cycle, E_{g}, will be presented in the following sub-section. In order not to "overload" the content of this article, we elect not to report diagnostic measurements

other than electrical ones (I, V, and their dependence on time, t, and frequency, f); the interested reader may find other types of diagnostic measurements, for example (gas) temperature [8] and optical emission spectroscopy [15] in other publications from this laboratory.

Table 4.1 Relative permittivities (κ'_{die}) and thickness (d_{die}) of dielectrics used in this research.

Dielectric Barrier Material	$\kappa'_{\mathbf{die}}$	$d_{\mathbf{die}}$ **(mm)**
Alumina (Al_2O_3)	9.5	2.0
Machinable Ceramic (Macor®)	6.0	2.0
Borosilicate Glass	4.0	2.0
Poly(tetrafluoro-ethylene) (Teflon®)	2.1	2.0

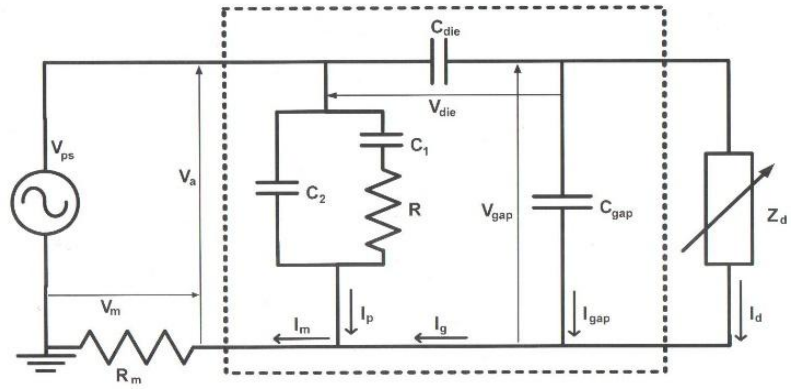

Figure 4.2. Equivalent electrical circuit diagram; the portion in the dashed rectangle represents the discharge cell. R_{m} = 50 Ω; see text for further details.

4.2.2 Equivalent Circuit Model and Energy Computation

Fig. 4.2 presents the equivalent electrical circuit model for both experimental set-ups, small and larger *A* DBD reactors, while the portion inside the dashed rectangle corresponds only to the actual discharge cell. V_{ps} and V_{m} correspond to the voltage signals respectively measured by the aforementioned high- and low-voltage probes. R_{m} is a 0.1% precision 50 Ω resistor, Z_{d} is a non-linear variable impedance; its value, although unknown with precision, tends toward zero during discharges and toward infinity between discharge events.

In both cases, parameters C_1, C_2, C_{die}, C_{gap}, and R were derived from separate sets of nominally identical V_{ps} and V_{m} measurements, but obtained when the cells were open to atmospheric air and therefore no discharges were present on account of the high breakdown voltage of air. From these V_{ps} and V_{m} measurements, $I_{\text{m}} = V_{\text{m}}/R_{\text{m}}$ and $Z_{\text{eq}} = V_{\text{a}}/I_{\text{m}}$ were calculated. These sets of V_{ps} and V_{m} measurements in air without discharges were repeated for frequencies, f, varying from 0.5 up to 40 or 50 kHz. As shown in Fig. 4.3, the amplitudes and phases of Z_{eq}, when plotted as a function of f for typical scenarios, quite precisely follow the theoretical response corresponding to the model, Fig. 4.2, over the entire frequency range.

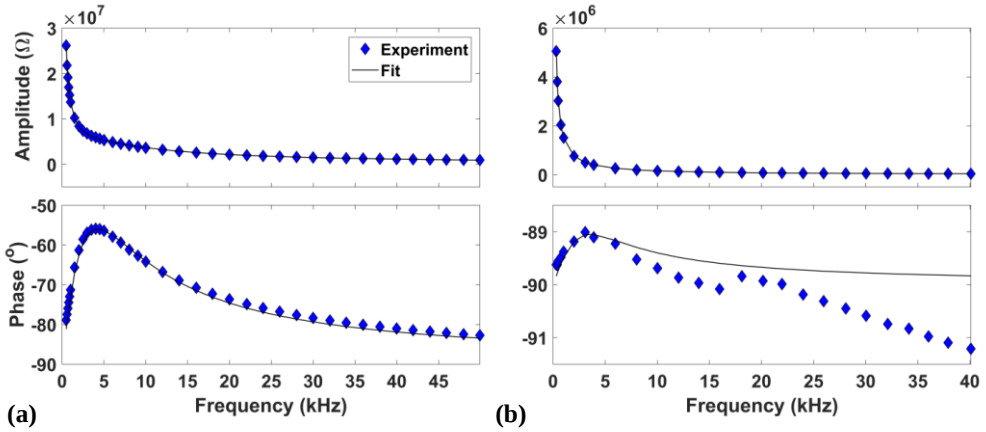

Figure 4.3. Characteristics (amplitude and phase) of the (a) small; and (b) large DBD reactors, as a function of frequency, f, of the same applied a.c. voltage (V_{a}) as during He or Ar discharges (measured at 100 kPa in air, where no discharges are present). The continuous curves through the data points represent the best fits to the presented equivalent circuit model. In (b), notice that deviations in phase angle are only about 1°.

Fig. 4.3 shows graphical comparisons with experimental data points for both the small (a), and large (b) DBD reactors; the best fits obtained from the equivalent C_1, C_2, C_{die}, C_{gap}, and R models are quite remarkable. Knowing the dimensions of the dielectrics, the gap spacing and the relative permittivities κ'_{die} of the dielectric materials, C_{die} and C_{gap} can be calculated. Table 4.2 summarizes numerical values corresponding to Fig. 4.3 for both the small and large reactors. Not unexpected, the phase angle in (a) varies widely (from ca. 55 to 82° between 3 and 50 kHz), while that in (b), between 89 and 91° in the same frequency range, deviates little from 90°, which

corresponds to the ideal response anticipated for this large-area planar, low-loss capacitor. We shall return to these characteristics later in the text.

Table 4.2 Values of the equivalent circuit model elements, Fig. 3.*

DBD reactor	C_1 **(pF)**	C_2 **(pF)**	C_{die} **(pF)**	C_{gap} **(pF)**	R **(MΩ)**
Small	8.80	1.41	18.1	2.34	7.95
Large	3.30	43.7	143.2	95.6	16.9

*Values for the small reactor pertain to *alumina* dielectric; large reactor: Macor® + glass (invariable).

By applying Kirchhoff's laws to the equivalent circuit in Fig. 2, the following equations are obtained:

The voltage across the cell V_a is given by:

$$V_a = V_{ps} - V_m. \tag{4.5}$$

The measured current I_m corresponds to:

$$I_m = \frac{V_m}{R_m}. \tag{4.6}$$

To calculate the gas current I_g, we need to compute the parasitic impedance Z_p and current I_p:

$$Z_p = \frac{1}{i\omega C_2 + 1/(R + 1/i\omega C_1)}, \tag{4.7}$$

$$I_p = \frac{V_a}{Z_p}, \tag{4.8}$$

$$I_g = I_m - I_p. \tag{4.9}$$

Computing the dielectric impedance Z_{die} is required to calculate the voltage across the gap, V_{gap}:

$$Z_{\mathrm{die}} = \frac{1}{i\omega C_{\mathrm{die}}}, \tag{4.10}$$

$$V_{\mathrm{gap}} = V_{\mathrm{a}} - I_{\mathrm{g}} Z_{\mathrm{die}}, \tag{4.11}$$

Calculating the gap current I_{gap} requires first to compute the gap impedance, Z_{gap}:

$$Z_{\mathrm{gap}} = \frac{1}{i\omega C_{\mathrm{gap}}}, \tag{4.12}$$

$$I_{\mathrm{gap}} = \frac{V_{\mathrm{gap}}}{Z_{\mathrm{gap}}}. \tag{4.13}$$

The discharge current I_{d} is obtained by:

$$I_{\mathrm{d}} = I_{\mathrm{g}} - I_{\mathrm{gap}}. \tag{4.14}$$

Finally, the electrical energy dissipated in the gas discharge per cycle, E_{g}, is:

$$E_{\mathrm{g}} = \frac{\int V_{\mathrm{gap}} I_{\mathrm{d}} dt}{n}. \tag{4.15}$$

Here n is the number of complete cycles at the applied voltage frequency.

4.3 Experimental Results and Discussion

Fig. 4.4 (a) to (d) present typical examples of measured (V_{a}, I_{m}) and calculated (V_{gap}, I_{d}) electrical signals obtained in the large DBD reactor for the cases of noble gas discharges, respectively He (a, b) and Ar (c, d), under the listed experimental conditions. While (a) shows the well-documented features of APGD in He gas [18, 25], namely single, short-duration (< 5 μs) current peaks per a.c. half-cycle, (b) also manifests "glow" behavior in He at higher V_{a}, where multiple discharge peaks occur per half-cycle, termed "pseudoglow" by Radu et al. [7]. Clearly, the DBD here occupies a much larger fraction of the a.c. half-period. According to the literature, Ar DBD is expected to be *filamentary*, unless the Ar is "doped" with certain vapors or gases such as a ketone like acetone, or ammonia [25]. While, in the small reactor, filamentary behavior did prevail with pure Ar, in the large reactor, very similar characteristics as for He (a, b) could be observed for *pure* Ar under practically all experimental conditions [see Fig. 4.4 (c, d)]. Experience in our laboratory has also shown that all but a few highly electronegative "dopant"

additives result in APGD-type behavior like that in (c, d), including O_2 [16]. To the best of our knowledge, these observations for the case of Ar DBD are so far unreported by others.

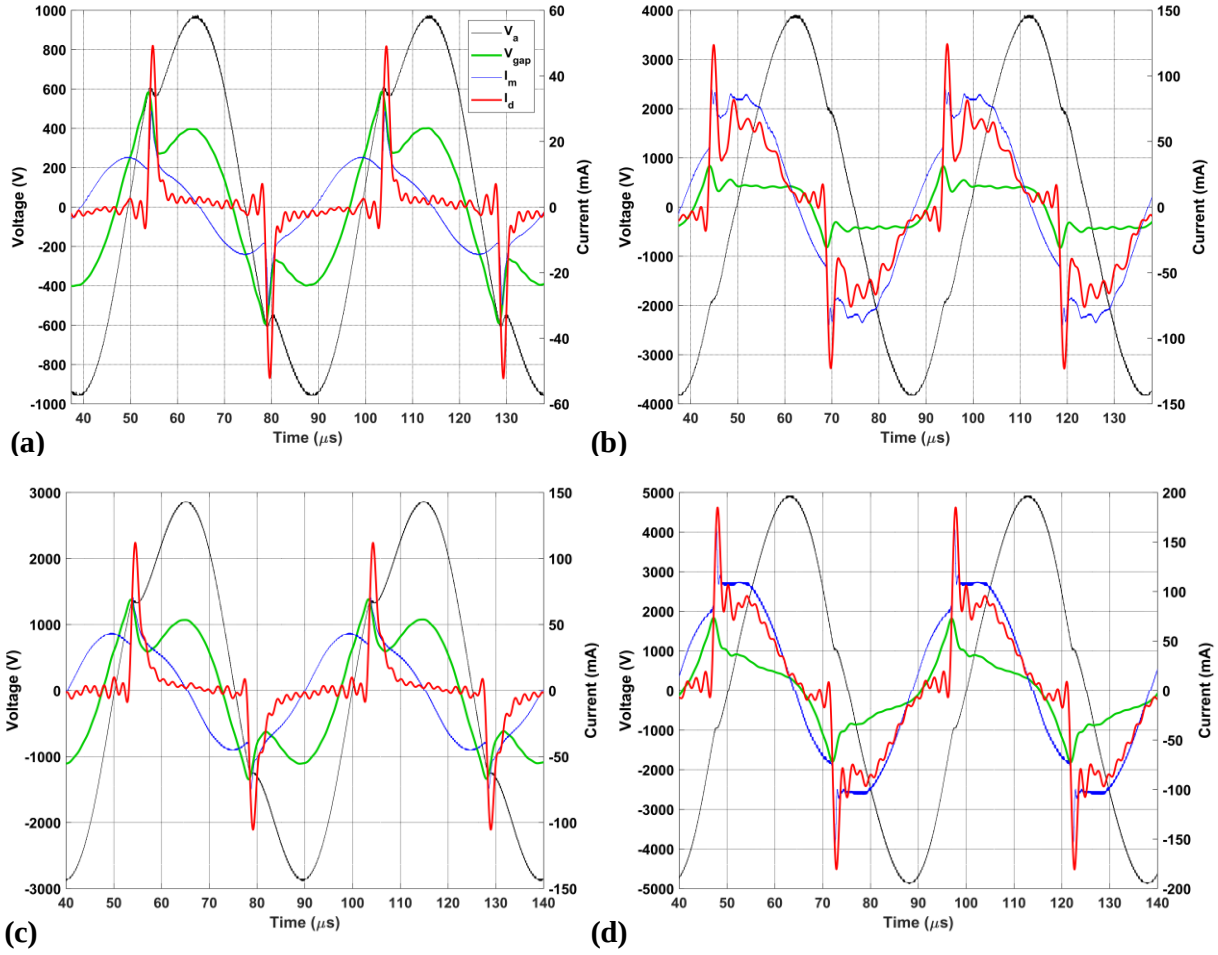

Figure 4.4. Typical examples of measured (V_a, I_m) and calculated (V_{gap}, I_d) electrical signals of multiple (two) periods of DBD in the large reactor: (a, b) APGD in He (f = 20 kHz, d_{gap} = 2 mm); (a) V_a = 675 V_{rms}: (b) V_a = 2.8 kV_{rms}; (c, d) APGD in Ar (f = 20 kHz, d_{gap} = 2 mm); (c) V_a = 2.0 kV_{rms} ; (d) V_a = 3.3 kV_{rms}. The characteristics of the large reactor, for example the dielectric barrier materials, are described in sub-section 4.2.1.

Using eq. (2), it is possible to evaluate the energy dissipated per cycle of the applied a.c. voltage, as illustrated in Fig. 4.5 for the case of He discharges in the *small* reactor, where different pairs of dielectric barrier materials have been utilized.

Fig. 4.5 shows "quasi-linear" increases in E_g with rising V_a, albeit with differing "slopes" and over different V_a ranges. These quasi-linear characteristics are not unexpected, considering the continuous "APGD-like" behavior of He with rising V_a as described in Fig. 4.4. Nevertheless, the main feature of Fig. 4.5 that we wish to underline here is the following: while the Al_2O_3 dielectric permitted experimentation over a wide range of V_a values, this was not the case for the other materials because arcing tended to occur at higher V_a. This can be explained by the fact that a lower voltage drop occurs at the dielectric materials and, therefore, a larger proportion of V_a is present at the gap when using materials with higher relative permittivities, κ'_{die}. The set-up is therefore more efficient at applying higher voltages through the gap for a given applied voltage V_a when using higher-κ'_{die} materials. It also emerges clearly that at any given V_a, values of E_g rise almost proportionately with κ'_{die}; this is illustrated in Fig. 4.5 by the superposed plot of E_g versus κ'_{die} for the case of V_a = 800 V_{rms}. This is the first such experimental demonstration, to the best of our knowledge [8].

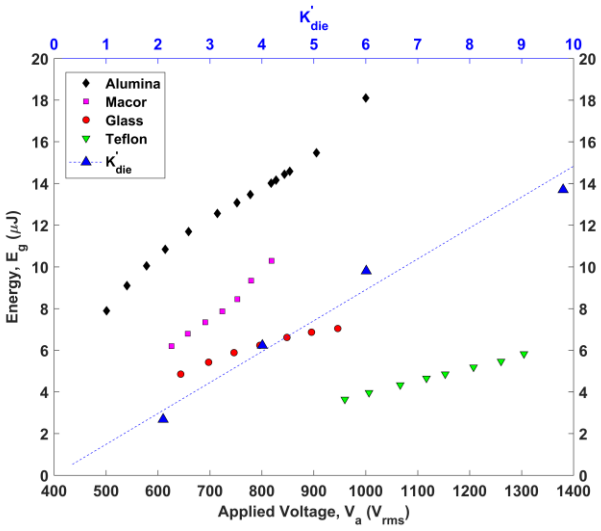

Figure 4.5. Plot of E_g versus V_a (Vrms) for He APGD at f = 20 kHz in the small reactor; different dielectric barrier materials of the same thickness, d_{die} = 2.0 mm, gap width, d_{gap} = 2.0 mm, and He flow, F = 3.1 L/min, were maintained constant throughout. The uncertainty of E_g values is estimated at < 10%, on the basis of multiple repetitions. The superimposed straight-line plot of E_g versus κ'_{die} represents values at V_a = 800 Vrms, which for PTFE (Teflon®) was obtained by downward extrapolation.

Capacitive edge and other parasitic effects dominated electrical behavior of the small reactor, as illustrated by the phase angles presented in Fig. 4.3, while this was clearly not the case for the large reactor. To test this hypothesis, we first calculated and plotted V_{gap} versus V_{a} data for the large reactor in Fig. 4.6 (a), then E_{g} versus V_{gap} in (b), for both He and Ar DBD. Note that the values of V_{gap} being discussed here correspond to the maximum values of the green-colored traces in Fig. 4.4.

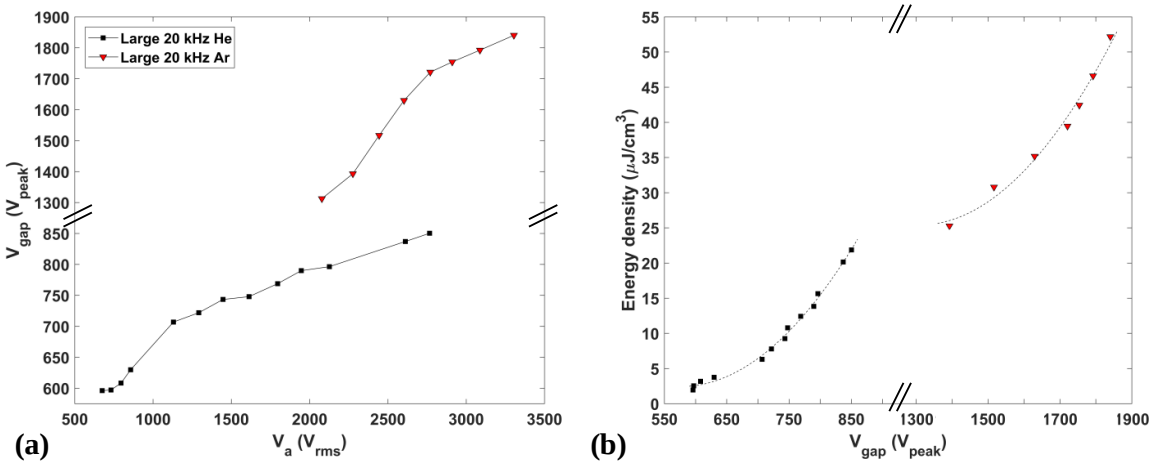

Figure 4.6. (a) Plots of V_{gap} versus V_{a}, and (b) of E_{g}/v versus V_{gap} for He and Ar DBD measurements conducted using the large reactor, where v is the plasma volume and the dielectrics are specified in the sub-section 4.2.1. In (b), the dotted line corresponds to a quadratic fit.

Several important observations can now be made on the basis of Fig. 4.6: First and foremost, the most relevant value of voltage that ought to be considered for characterizing DBD physics is V_{gap} rather than V_{a}, and the relationship between these two is clearly quite non-linear [see (a)]. Indeed, the plot of E_{g}/v versus V_{gap}, Fig. 4.6 (b), is here seen to display a quadratic behavior for both He and Ar DBD.

It is also of interest to examine a possible relationship between energy stored in the dielectrics and gap capacitors (eq. (4.1)) and E_{g}, the energy dissipated in the DBD plasma. If we recall the physics of an ideal (lossless) capacitor fed by an applied sinusoidal voltage, power $P_{\mathrm{i}}(t)$ at any instant t of the voltage period is given by:

$$P_{\mathrm{i}}(t) = V(t)I(t) = V(t)\frac{dQ(t)}{dt} = V(t)\left(C\frac{dV(t)}{dt}\right) = CV(t)\frac{dV(t)}{dt}. \tag{4.16}$$

Integrating over a full cycle yields a net value of zero, because energy stored in the capacitor by the power source during the first quarter-period is returned in full during the second, and the same process repeats for the third and fourth quarter-periods, but with the opposite voltage polarity. Thus, one can estimate the maximum value of energy stored in the capacitors (dielectrics and gap) by integrating over the first quarter-period, where the positive discharge occurs. Taking the lowest peak values of V_{a} presented in Fig. 4.6, namely 955 and 3220 V_{peak} in He and Ar, respectively, and using eq. (4.1), we compare calculated and measured energy densities per half-period, $E_{\mathrm{g}}/(2v)$, where v = 43.2 cm^3 is the plasma volume. The dielectrics in the large reactor were comprised of two different materials: glass (κ'_{die1}= 4.0, d_{die1} = 3.0 mm) and Macor® (κ'_{die2}= 6.0, d_{die2} = 3.5 mm). The parameters for the gap in the large reactor were: $\kappa'_{\mathrm{gap}}\approx$ 1.0, d_{gap} = 2.0 mm, and A = 216 cm^2. Respective numerical values of $E_{\mathrm{g}}/(2v)$ for He and Ar calculated using eq. (4.1), 0.30 and 3.44 μJ/cm^3, are roughly 3 and 4 times smaller than corresponding measured values of $E_{\mathrm{g}}/(2v)$ in Fig. 4.6 (b), ca. 0.95 and 12.6 μJ/cm^3, respectively. The obvious conclusion is that, while the discharge is active, most of the energy is provided by the a.c. power supply. However, it is interesting to compare those values from eq. (4.1) of energy stored in the dielectric and gap capacitors with what we shall call the "*power boost*" that can be observed in Fig. 4.4; this occurs when the discharge is initiated and the associated current I_{d} is larger than the measured current I_{m} coming from the a.c. power supply. The energy density of this "*power boost*" can be estimated by integrating over the period when $I_{\mathrm{d}} > I_{\mathrm{m}}$ using the following formula:

$$E = \int V_{\mathrm{gap}}(I_{\mathrm{d}} - I_{\mathrm{m}})dt, \quad \text{when } (I_{\mathrm{d}} - I_{\mathrm{m}}) > 0. \tag{4.17}$$

Using the same data as for the preceding calculation, eq. (4.4) yields respective values for He and Ar of 0.29 and 0.88 μJ/cm^3. These are clearly comparable with the ones presented above (0.30 and 3.44 μJ/cm^3); this supports our hypothesis that observed $I_{\mathrm{d}} > I_{\mathrm{m}}$ values at discharge

initiation result from energy stored in the combined dielectrics and gap capacitance. It is also interesting to compare energy dissipation in the small and large DBD reactor plasmas, but this must obviously be done with much caution. In the small reactor, Ar gave rise to fairly short-duration, triangular-shaped current peaks, but with superimposed filamentary current spikes, as also reported by Tyata et al. [13]. As V_a was raised, the filaments increased in numbers and amplitudes, particularly following the peak. On account of this and the higher breakdown strength of Ar, we had to reduce the gap width to d_{gap} = 0.5 mm but found E_g = 9 μJ per period at 20 kHz, V_a = 955 V_{rms}. The corresponding value of E_g/v = 36 μJ/cm^3 falls within the range 25 ≤ E_g/v ≤ 53 μJ/cm^3 for Ar in Fig. 4.6 (b), numerical agreement that may be considered satisfactory under the circumstances. This might help demonstrate the feasibility of transferring information from a small laboratory-scale to a much larger reactor, for example when planning scale-up to an industrial reactor system. As mentioned in the *Introduction* section, only few comparable reliable data can be found in the literature, and these apply exclusively to the case of He (APGD) DBD, namely those of Decomps [10] and Nersisyan [11]. Confronted with our own E_g/v measurements, especially the values 3 ≤ E_g/v ≤ 20 μJ/cm^3 in Fig. 4.6 (b), the respective values of 14 and 10 μJ/cm^3 are comparable. It should be mentioned that differences in dielectric compositions and thicknesses had to be compensated in order to enable these comparisons. Clearly, the agreement here is also acceptable, considering the quite different experimental setups used in the three laboratories, and the fact that this type of comparison appears to be without precedent in the literature.

Another interesting and entirely novel "spinoff" result comes in the form of breakdown fields of the four gases that have been investigated, He, Ne, Ar and N_2. Remember that precise numerical values of V_{gap}, the gap voltage at the instant of DBD initiation (see voltage and current peaks in Fig. 4.4 (a) to (d)), results from Matlab® code calculations under the various experimental conditions (different dielectrics, gap widths, etc). It is gratifying that breakdown field values, $F_b = V_{gap}/d_{gap}$, were found to be remarkably consistent throughout this study: In Table 4.3, present values are compared with corresponding ones from the literature. Regarding the latter, Christophorou [57] tabulated breakdown fields of several gases referenced to SF_6 (≡ 1.0), with the exception of He. One notes quite good agreement between current and literature

values of F_b, especially if one accounts for wide variations in the literature for a given gas, which may depend on secondary electron emission from different electrode surfaces, among numerous other variables. The fact that breakdown can occur at over-voltages that may very significantly exceed the lowest V_{gap} values in Fig. 4.6 (a), 596 and 1393 V_{peak} for He and Ar, respectively, is well documented in the literature, both for molecular gases such as nitrogen [58], as well as for noble gases [59]. In their article entitled "*Generalized Paschen's Law for Overvoltage Conditions*", Babich and Loiko show that with increasing "high-voltage waveform (HVW) steepness", achieved voltage amplitude $U(pd)$ increases above $U_{st}(pd)$, where U_{st} is the static self-breakdown voltage associated with the conventional Paschen plot, $d = d_{gap}$ and p is gas pressure [59].

It is noteworthy that, in Table 4.3, the only significant deviation between the present and literature values of F_b is observed in the case of Ne. We can only speculate about the reason for this, but for reasons of high cost, Ne was examined only in the *small* reactor, where it was found to be particularly prone to degradation of the discharge mode from "APGD" to streamers.

Table 4.3 Dielectric breakdown field values calculated from $F_b = V_{gap}/d_{gap}$, at f = 20 kHz. values from the literature are presented for comparison ([a] : large reactor; [b] : small reactor).*

Gas	**F_b (kV/cm) (present work)**	**F_b (kV/cm) (literature)**	**Frequency (kHz) (literature)**
He [a]	3.0	2.7 [10, 11]	50
Ne [b]	1.8	0.6 [57]	50
Ar [a]	6.9	7.0 [57]	20
N_2 [b]	37	36 [57]	7

* V_{gap} for He and Ar correspond to the lowest peak values for discharge initiation in Fig. 6.

4.4 Conclusions

We have used two home-designed and -built dielectric barrier discharge (DBD) reactors, one small, the other about 40 times larger, and associated equipment to carry out precise measurements of electrical energy, E_g, dissipated per discharge cycle of the applied a.c. voltage,

V_a. In the smaller reactor, this has been done over a broad frequency range $5 \leq f \leq 50$ kHz, using twin pairs of several different dielectric materials (2.54 cm diameter discs) with relative permittivities between $2.1 \leq \kappa'_{die} \leq 9.5$ as barrier materials in DBDs of four different gases: He, Ne, Ar and N_2. Here, we have presented mainly He and Ar data.

In the larger reactor, f was restricted to 20 kHz DBD in flowing Ar or He; this moveable substrate system has been designed primarily for plasma polymerization experiments in which ‰ concentrations of organic "monomers" are admixed with the 10 slm flow of pure Ar carrier gas, used instead of He for reasons of lower cost. A first surprising innovative result has been that, contrary to what was observed in the small reactor and reported in the literature, pure argon manifested non-filamentary "glow-type" behavior quite similar to that of helium in the large one. This can have important benefits for industrial implementation, particularly the fact that "APGD"-like behavior in Ar is promoted by many "dopant" gases and vapors other than the few (NH_3, ketones) so far reported in other literature [25].

We have brought additional proof through the fact that our novel method, which also allows one to determine gap voltage (V_{gap}) and true discharge (I_d) current, hence E_g, completely overcomes problems with traditional methods like Lissajous figures, which are prone to serious pitfalls [35]. The method, assisted by its own dedicated Matlab® code, is so far used only in this laboratory. To the extent possible, E_g values were compared between the small and large reactors, and with related results in the literature. Data obtained with the larger reactor are deemed more reliable on account of its much-reduced parasitic edge effects, novel and clearly evident from the frequency responses in Fig. 4.3(a,b).

The correctness and reliability of E_g and related measurements has been further verified by several other independent means; for example, dielectric breakdown fields, F_b, of the four gases examined could be calculated using V_{gap} values derived from our Matlab® model, and these were found to agree well with data from the literature [57]. Elsewhere [8], we had already shown that calorimetric measurements based on E_g values in He led to good overall energy balance results, another clear and unambiguous evidence for the method's validity. Lastly, this methodology also allowed us to elect V_{gap} as the most relevant voltage value to be considered for characterizing DBD physics, and to point out its non-linear relationship with the *applied* voltage, V_a.

In summary, this research contributes several new insights, for example those listed above, into the physics and technology of dielectric barrier discharges, a field that is presently experiencing enormous growth in pure and applied plasma science and technology.

Acknowledgments: Skilled technical help by Mr. Yves Leblanc is gratefully acknowledged, as are grants from NSERC and FRQNT.

CHAPTER 5 ARTICLE 2: ENERGETICS OF REACTIONS IN A DIELECTRIC BARRIER DISCHARGE WITH ARGON CARRIER GAS: VIII HYDROFLUOROMETHANES

Sean Watson, Bernard Nisol, Michael R. Wertheimer

Article published in:

Plasma Processes and Polymers, 2019, *early view*, e. 1900125.
https://doi.org/10.1002/ppap.201900125

Energetics of Reactions in a Dielectric Barrier Discharge with Argon Carrier Gas: VIII Hydrofluoromethanes

Abstract— The method we have developed for understanding energetic exchanges between precursor molecules and Ar carrier gas in a dielectric barrier discharge (DBD) has much proven merit. The present article focuses on hydrofluoromethanes, CH_xF_y. Precursors (‰ concentrations) were mixed with Ar in a 20 kHz, 8 kV (peak-to-peak) DBD. For each compound, E_m, the energy absorbed per molecule, was plotted as a function of precursor flow rate. Beside determination of E_m, we have used optical emission spectroscopy as a diagnostic of the plasma physico-chemistry. The influence of chemical structure has been investigated by depositing thin plasma polymer coatings; we have measured their deposition rates and water contact angles, which have been correlated with E_m values and XPS measurements.

5.1 Introduction

The present research constitutes an entirely new addition to a series of earlier-published investigations based on a powerful, original methodology developed in this laboratory for measuring energetics of reactions in a DBD with Ar carrier gas at AP.

Atmospheric-pressure plasmas have been receiving much attention during recent decades, and they are already used in numerous applications including surface functionalization and the synthesis of various coating-types by PECVD [30, 60]. The absence of vacuum systems is an important advantage, which may render AP economically more viable for industrial uses [2, 25, 30]. HV DBD reactors, using one or more electrodes covered by a dielectric layer and separated by a small (~ mm) gap, are a preferred approach because they can be scaled up quite readily [18]. Of course, in the case of PECVD, physico-chemical properties of AP PP coatings will strongly depend on the nature of the monomer/precursor gas or vapor.

In spite of the now extensive body of published research, understanding the fundamental mechanisms involved remains elusive. The so-called Yasuda parameter (W/FM) [39, 53] from the late 70's, where W, F and M respectively represent the applied discharge power, monomer/precursor flow rate and mass, was proposed to help unravel LP plasma polymerization/fragmentation mechanisms. Although useful to some limited extent, it has major

shortcomings under AP conditions: here, the monomer is usually diluted in an inert carrier gas (He or Ar), which totally changes the energy transfer mechanisms. Indeed, such AP plasmas are not only driven by inelastic electron collisions, like in the LP case, but mainly by Penning-transfer via excited metastable inert carrier gas atoms [18]. The present authors have developed a technique for evaluating this energy transfer by way of electrical [voltage, $V(t)$ and current, $I(t)$] measurements when a monomer flow, F_{d}, is added in ‰ concentration to the much greater Ar carrier gas flow [9, 15, 16]. The resulting parameters, ΔE_{g} and E_{m}, respectively represent energy absorbed from the plasma by F_{d}, per monomer molecule, and per duration of the applied a.c. voltage period. This has enabled us to observe the effect of slightly modifying the chemical structure of molecules within various families of monomers and precursors, for example in references [15-17, 56, 61].

There now exists an abundant body of evidence that supports not only the methodology for evaluating ΔE_{g} and E_{m}, but also numerical values derived therefrom for cases of specific precursor molecules. Here are three sample-items from among that list of supporting evidence:

1) In ref. [9], ΔE_{g} and E_{m} were first examined for a simple hydrocarbon, CH_4, where it was found that results were highly reproducible and independent of V_{a} and f (within certain obvious limits). In that same paper, it was also found that E_{m} ~ 9 eV for C_2H_2, the exact literature value of that molecule's bond strength.

2) In another paper [56], it was reported that E_{m} rose linearly with rising molecular weight, M, for the case of the family of saturated hydrocarbons, from C_1 up to C_8.

3) In a series of three collaborative articles, jointly with D. Hegemann [62-64], values of E_{m} derived using the DBD-based methodology could be favorably compared with the outcomes of low-pressure r.f. plasma-based experiments using Hegemann's well-known macroscopic methodology [49].

The authors admit that detailed mechanisms giving rise to ΔE_{g} when reactive precursor molecules are added to pure Ar carrier are complex and only partly understood; some hints may nevertheless be drawn from modeling studies like the one recently published by Loffhagen *et al.*[65] However, it is clear that overall conditions prevailing in the DBD plasma must then rapidly

equilibrate and stabilize, distinct from those in pure Ar, whereby the physico-chemistry in the "mixed gas" discharge obviously governs the experimentally-observed outcomes.

In this present article, the eighth of a series in this same journal, special attention was given to the importance of hydrogen/fluorine ratio in the family of five hydrofluoromethane compounds, CH_xF_y ($0 \leq x \leq 4$; $y = 4 - x$). The shapes of the E_m curves for each different molecule as a function of F_d will be discussed and correlated with optical emission spectroscopy (OES) as a diagnostic of the plasma physico-chemistry, along with deposition rates, water contact angles and chemical compositions of the resulting PP coatings, the latter determined by X-ray photoelectron spectroscopy, XPS. From a practical point of view, fluorocarbon precursors have always been important in plasma chemistry [66, 67] because they can give rise to "poly(tetrafluoroethylene), PTFE-like" surfaces and coatings, also in AP DBD reactors [68-73]. To the extent possible, the present results are compared with those earlier publications.

5.2 Experimental Section

A complete description of the DBD reactor and its electrical power supply used in this study can be found in references cited above. Nevertheless, it is useful to repeat certain important technical aspects below. The large-area (A = 216 cm^2) planar DBD system had a 2 mm-wide gap between the upper (Macor® ceramic, 3.50 ± 0.05 mm thick) and lower (glass, 3.00 mm ± 0.02 mm) dielectrics. The plasma was sustained at fixed audio-frequency, f = 20 kHz, and peak-to-peak applied voltage, V_a = 8 kV (2.8 kV_{rms}). The flow rate of Ar carrier gas (99.99% purity, Air Liquide Canada Ltd, Montréal) was kept constant, F = 10 standard L/min (slm). The five gaseous precursors, methane (CH_4), perfluoromethane (CF_4), and their hydrofluorocarbon intermediates (CH_3F, CH_2F_2, and CHF_3) were used as received (from SynQuest Laboratories, Inc., FL, USA). Varying known amounts, F_d, measured with an electronic gas flow meter/controller (MKS, type 1259B, 0-100 sccm), were admixed with the 10 slm Ar carrier gas flow. This was accomplished by merging the two gas flows, 10 slm of Ar, and F_d of hydrofluorocarbon, in a mixing chamber upstream of the diffuser that then injected the mixture into the interelectrode gap space.

Using the earlier-reported equivalent circuit model and MATLAB® program, we determined E_g (in μJ), the energy dissipated in the AP DBD plasma during each applied a.c. HV cycle. The

energy difference, ΔE_g, associated with precursor admixture was evaluated for wide flow ranges, $0.1 \leq F_d \leq 70$ sccm depending upon the particular precursor, which in turn permitted calculation of E_m (in eV). Resulting AP discharge plasmas and PP coatings, where applicable (CF_4, a well-known etchant, never gave rise to PP deposits, as discussed again later), were then characterized using the following techniques:

(i) Optical emission spectroscopy (OES) was carried out as a simple, non- invasive diagnostic technique, using a compact Ocean Optics USB-2000 spectrometer, coupled with a ø= 105 µm optical fiber. The accessible spectral range was ca. 250-800 nm, and measurements were carried out as a function of precursor flow rate, F_d. Light emitted from the 2 mm wide DBD gap was captured by the optical fiber, protected from active plasma species by a thin quartz-glass plate. The fiber was positioned 4 cm away from the plasma zone; of course, one fully expects the optical emission spectra to be spatially-dependent along the gas flow direction, just like the film deposition rate and -composition. Accordingly, the optical fiber was installed perpendicularly to the direction of gas flow (thereby collecting photons from a narrow 18 cm-long portion corresponding to the DBD plasma‘s width), but close to the point where the gas mixture was injected by the linear gas-diffuser. This assured that, even for the case of smallest F_d, these molecules had not appreciably been converted or depleted by reactions in the plasma. For the case of high F_d, this is not a source of concern because the depletion front moves increasingly further away from the diffuser, until the point where, at highest F_d, some of the precursor feed will leave the 6 cm-long DBD unreacted. These statements are supported by experimental results with HMDSO precursor [63].

Characterization methods used are described further below, but in all cases and under all experimental conditions the following procedure was adopted: a small (ca. 1 cm^2) piece of single-crystal silicon (c-Si) wafer was placed on the lower (grounded) electrode’s dielectric (glass) plate. During experiments, this 28 cm long electrode was displaced back-and-forth through the plasma zone at 15 mm/s so as to assure uniform exposure. Thereby, the c-Si surface witnessed the complete set of conditions encountered at its surface, averaged over the entire duration of the experiment.

(ii) Spectroscopic ellipsometry (SE) measurements were performed on PP-coated silicon wafer fragments using a J.A. Woollam RC2® instrument operating between 193 and 1700 nm. The Δ and ψ parameters were determined at 45°, 55°, 65° and 75° incidence angles; data were interpreted using the CompleteEASE™ software and a B-spline. Measured refractive index values were in the order of 1.5. Using thicknesses determined by SE, deposition rates, *r*, corresponding to the various PP coating conditions could then readily be determined.

(iii) XPS analyses were carried out in a VG ESCALAB 3 MKII spectrometer. Spectra were acquired using a Mg anode (1253.6 eV) operating at 300 W. The pass energy was set to 100 eV for survey spectra (not presented here), and 20 eV for high-resolution (HR) C 1s peak shape analysis. The high resolution C 1s peak fitting was performed using CasaXPS (CasaSoftware Ltd.), by considering the lowest number of physically meaningful components; for the sake of clarity, these were restricted to the "first neighbor"-induced chemical shift (C–C/C–H, C–N/C-O, C*-CF_x, C-F, C-F_2) [74, 75]. The FWHM (20 eV pass energy) of these components was constrained to 1.8 ± 0.1 eV, and binding energies were charge-referenced by setting the hydrocarbon (C-C/C-H) component to 285.0 eV.

(iv) Contact Angle Goniometry (CAG), using milliQ (ultrapure) water, static contact angles of 2 μl droplets were measured on five different areas of the coated c-Si surfaces; the instrument was a Ramé-Hart goniometer (model 100-00).

5.3 Results and Discussion

5.3.1 Energy Absorbed by Precursor Added to the Ar Carrier Gas

The electrical energy, E_g, dissipated in the gas discharge during each applied HV cycle was

$$E_g = \frac{\int V_{gap} I_d dt}{n} \tag{5.1}$$

where n is the number of complete cycles at frequency, f. The reader is referred to references [8, 9] for other details, so these will not be repeated here.

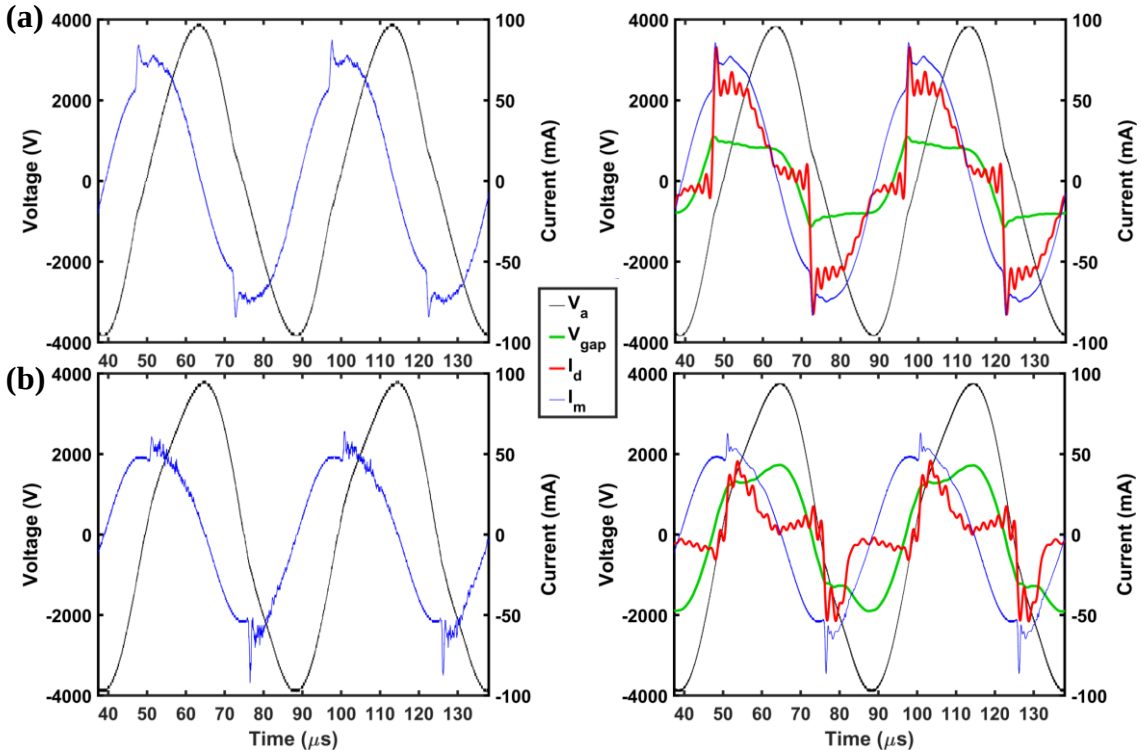

Figure 5.1. *Right-hand side*: Examples of measured (V_a, I_m) and calculated (V_{gap}, I_d) electrical signals of two DBD periods, averaged over one minute of data acquisition: (a) APGD in Ar + 30 sccm of CH_4 (f = 20 kHz, d_{gap} = 2 mm; V_a = 2.8 kV_{rms}); (b) APGD in Ar + 32 sccm of CF_4, same DBD conditions. *Left-hand side*: "instantaneous" (ca. 50 μs) V_a and I_m signals, showing more filamentary nature of (b).

Figure 5.1 presents typical examples of measured (V_a, I_m) and calculated (V_{gap}, I_d) waveforms of AP DBD plasmas in flowing Ar, F = 10 slm, f = 20 kHz, V_a = 2.8 kV_{rms} (= 8 kV_{p-p}), in two different cases where the Ar flow included (a) F_d = 30 sccm of methane (CH_4); and (b) F_d = 32 sccm of perfluoromethane (CF_4). It is noteworthy that $I_d(t)$ was continuous, albeit with some peaks, and that its duration, ~20 μs, corresponded to nearly 75% of the $V_a(t)$ half-period. According to the literature, Ar DBD is expected to be *filamentary*, unless the Ar is "doped" with certain vapors or gases such as a ketone like acetone, or ammonia [25]. While in a smaller-area (A = 5.1 cm^2) DBD reactor in this laboratory, filamentary behavior did prevail with pure Ar, in the present large-area (216 cm^2) reactor "AP glow-discharge (APGD)-like" behavior, much like that in pure He, could be observed for *pure* Ar under all experimental conditions [76], even when the

Ar was "doped" with an electronegative gas such as O_2 [15]. Quite remarkably, this was even observed for the extremely electronegative CF_4 additive, as noted in **Fig. 5.1**(b): Although the short-duration (ca. 1 period, or 50 μs) oscilloscopic trace depicting I_m showed evidence of many rapid (ns) filamentary discharges per half-period (unlike its much "smoother" CH_4 counterpart), the time-averaged traces of I_m and I_d were smooth enough to permit reliable evaluations of E_g using eq. (5.1) above. This clearly emerges from the family of E_m vs $1/F_d$ plots in **Figure 5.2**, as well as from E_m vs F_d plots presented separately for each of the molecules in section 3.3 further below.

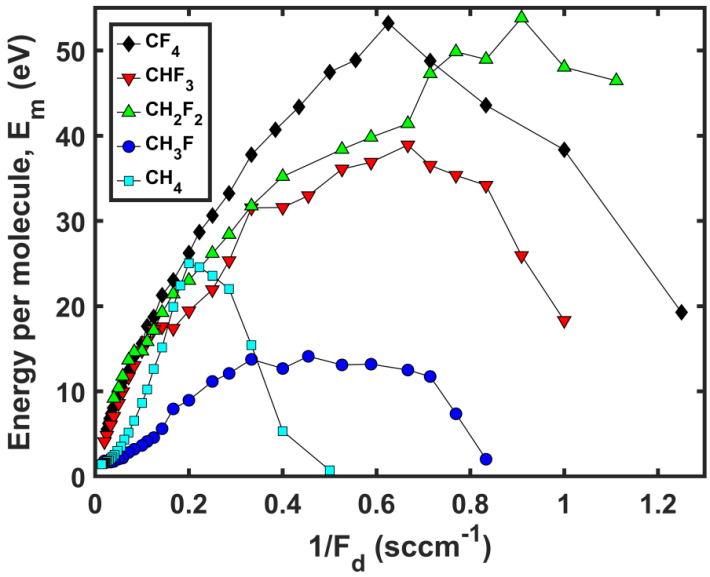

Figure 5.2. Plots of E_m versus $1/F_d$ (see text) for the five CH_xF_y molecules used in this research. Characteristics of particular interest, namely the values of $(E_m)_{max}$ and of the initial slopes, $[d(E_m)/d(F_d)]$, will be the objects of discussion later in this text.

5.3.2 Optical Emission Spectroscopy (OES)

Figure 5.3 presents a superposition of OE spectra covering the wavelength range between ca. 250 and 900 nm. Different colors, corresponding to specific experimental cases (see box), highlight the main spectral features that served in the following sections to discuss molecular fragmentations and likely chemical reaction pathways.

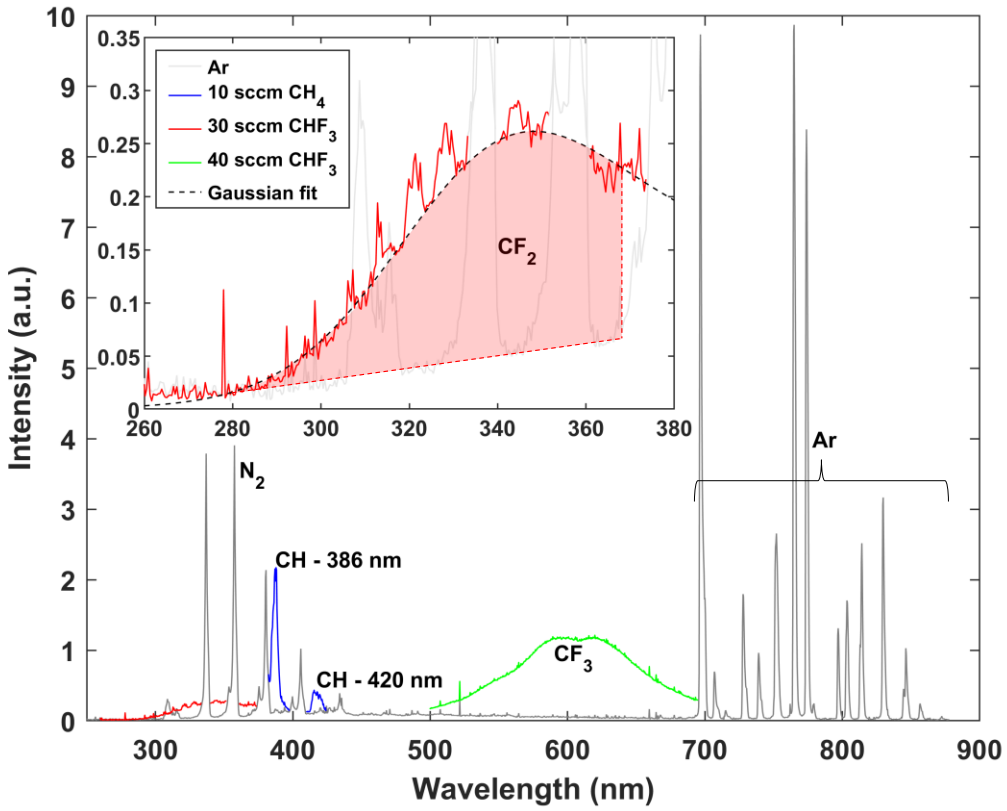

Figure 5.3. Optical emission spectra of Ar/CH_xF_y mixture DBD plasmas. Different colors, corresponding to specific cases (see box), highlight the main spectral features that served for diagnostics in the following sections.

The reader is referred to articles by Fanelli [71] and by Vinogradov and Lunk [68], authors who dealt in considerable detail with OES of DBD plasmas in Ar/CF_x gas mixtures. According to Fanelli, the very broad "CF_2" band (ca. 240-360 nm) can be attributed to contributions from CF_2, CF_2^+, and ArF_2 species, and she also reported $N_2(B)$ emissions from trace amounts of nitrogen, contamination that presumably arose from tiny air leaks (small enough that no O_2 contribution could be detected, for example at 777 nm). On the basis of Fanelli's observations, it might at first appear that our measured CF_2 spectra were red-shifted. However, for the case of LP C_2F_4 r.f. plasmas, Cruden *et al.* also reported and tentatively assigned their broad (240-380 nm) band to CF_2 [77].

Let us now explain how these spectra were used to obtain the semi-quantitative data presented in following sections: All measured spectrometric data (in units of "counts per

second") were normalized with respect to integration time (in milliseconds), instead of highest peak intensity, the latter usually employed by other workers. Nevertheless, after testing both methods and finding quite similar semi-quantitative results, we concluded that the first method above more readily permitted quenching phenomena to be distinguished, whenever these were observed.

First, turning to the CF_2 band, its measured intensity distribution within the wavelength range between ca. 278 and 370 nm was fitted either by a single Gaussian or the sum of two Gaussians, care being taken not to include spectral contributions from the overlapping N_2(B) lines (see **Fig. 5.3**). Using the (linear) baseline of a pure Ar emission spectrum, the area under the best-fit profile was then evaluated by integration; by way of example, the red highlighted inset in **Fig. 5.3** illustrates the semi-quantitative CF_2 contribution for a gas mixture comprising (Ar + 30 sccm CHF_3).

Regarding the other spectral features in **Fig. 5.3**, semi-quantitative contributions from hydrocarbon bands [383.8 to 391 nm (CH: $A^2\Delta \rightarrow X^2\Pi$ (0,0)) [78]; 412.6 to 424.1 nm (CH+: $^1\Pi \rightarrow {}^1\Sigma$ (2,1)][78] were obtained by direct integration of the (blue) highlighted areas. CF_3, illustrated in **Fig. 5.3** (green curve) for the case of emission from (Ar + 40 sccm CHF_3) gas mixture, manifested a very broad band centered near 610 nm, which was readily quantified by integration and again subtracting the Ar background contribution.

In the next section, we shall be presenting such semi-quantitative OES data for the various (Ar + CH_xF_y) gas mixtures in relation to their E_m/F_d values; in order to do so in a meaningful way, the intensity values determined via the above-described integrations were normalized with respect to the numbers of precursor molecules in the given mixture flows (multiplied by 10^{19}), thereby defining a new parameter *"intensity per molecule"*, J_m. This J_m parameter will serve to characterize OES data in the following sets of sub-sections.

5.3.3 Results for Individual Ar/CH_xF_y Mixtures

5.3.3.1 Ar/CF_4

Figure 5.4 (a) shows a log-log plot of E_m versus F_d for the case of Ar/CF_4 mixtures in the range $0 \leq F_d \leq 40$ sccm, while (b) represents OES "intensities per molecule", J_m (defined in the

preceding section 3.2) of the CF_2 and CF_3 bands, also on log-log scales, for the corresponding F_d values. The following observations can now be made: (i) The spectra did not display any of the "CH" features in **Fig. 5.3**, fully to be expected because the molecule contained no hydrogen.

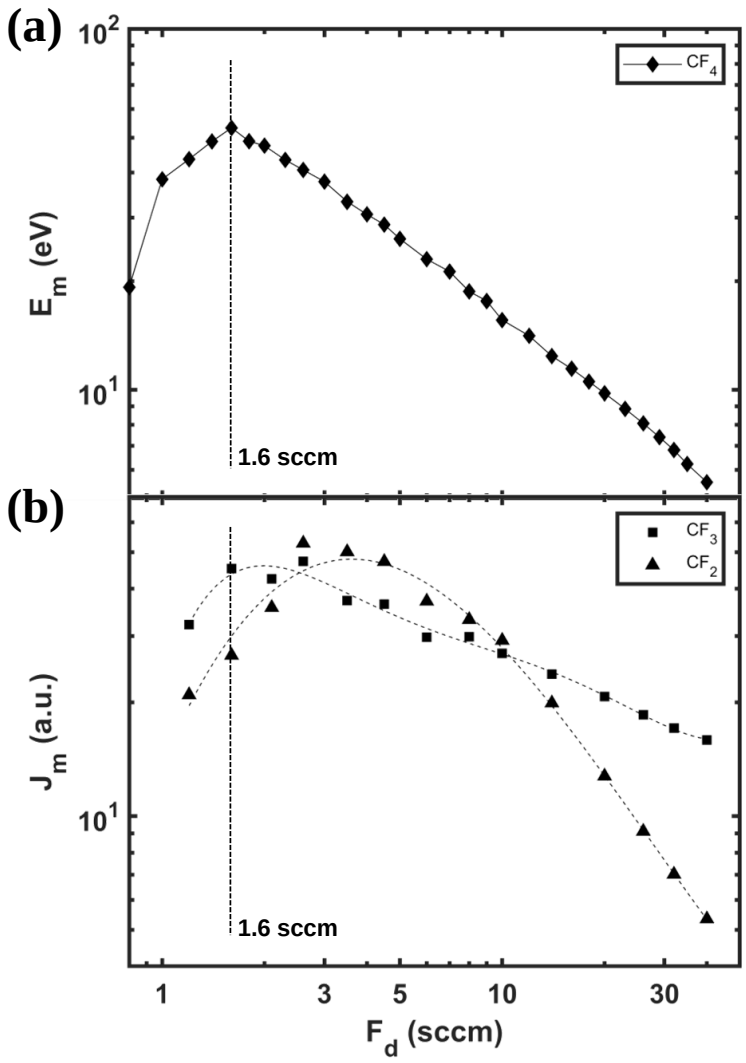

Figure 5.4. Plots of (a) E_m versus F_d; and (b) J_m versus F_d (see text for explanations), for the case of Ar/CF_4 mixtures with $0 \leq F_d \leq 40$ sccm (log-log scales, base 10).

(ii) Maximum values of J_m for CF_3 and CF_2 occurred at high E_m (low F_d), then systematically decreased, following the same trend as E_m. Indeed, the maximum intensity for CF_3 occurred precisely at $(E_m)_{max}$ (F_d = 1.6 sccm), while that of CF_2 was shifted towards slightly higher F_d. (iii) Strikingly, inspecting the (negative) slopes of J_m for CF_3 and CF_2 in the "*monomer"-rich*

region (F_d > 1.6 sccm), one notes that of CF_2 to be greater; this confirms that CF_2 formation was less favored at lower E_m (higher F_d). (iv) Finally, no PP deposition was ever observed, as expected for this strong plasma-etchant, CF_4; therefore, no deposition rate or XPS data are presented in this sub-section.

5.3.3.2 **Ar/CHF_3**

Figure 5.5 (a) shows a log-log plot of E_m versus F_d for the case of Ar/CHF_3 mixtures in the range $1 \leq F_d \leq 50$ sccm, while (b) represents J_m of the CF_2, CF_3 and CH (386 nm) bands, also on

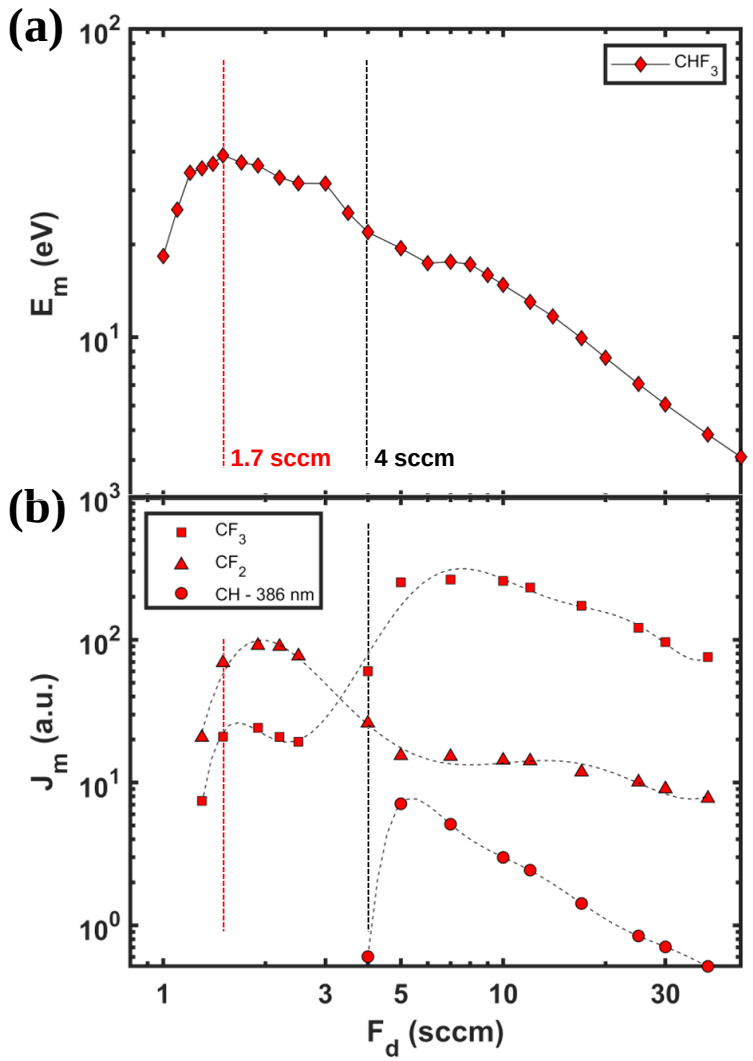

Figure 5.5. Plots of (a) E_m versus F_d; and (b) J_m versus F_d (see text for explanations), for the case of Ar/CHF_3 mixtures with $0 \leq F_d \leq 50$ sccm (log-log scales, base 10).

log-log scales, for the corresponding F_d values. As was done in the preceding sub-section, we can now make the following observations:

(i) CF_2 had a maximum near $(E_m)_{max}$ (F_d = 1.7 sccm), then dropped in remarkable accord with $E_m(F_d)$, while CF_3 presented a first maximum near $(E_m)_{max}$. (ii) A transition occurred at F_d = 4 sccm, at which CF_3 rose markedly while CF_2 dropped still further with decreasing E_m (rising F_d). No emission from CH could be detected below the 4 sccm transition, but for F_d > 4 sccm it rose to a sharp peak, then dropping with the same trend as E_m, as did the other emission intensities.

The following tentative conclusions emerge: to the left of the 4 sccm transition, it appears that conditions favored abstraction of an H and an F atom for each molecule; to the right (lower E_m), the inverted trends between CF_3 and CF_2 suggest greater difficulty to extract an F atom, while solely H removal continued unhindered. In view of C-H and C-F bond energies, 4.25 and 5.08 eV, respectively, this is not unexpected. Having stated this, the sudden appearance of CH indicated that even in the "*monomer"-rich* regime some molecules underwent greater degrees of fragmentation than that suggested only by the CF_3/CF_2 trend. Since CHF_3 (and the other CH_xF_y molecules discussed in following sub-sections) gave rise to PP film deposition, i.e. PECVD, we can now refer to XPS measurements that were conducted on these deposits. **Table 5.1** presents film compositions, based on broad-scan XPS measurements of CHF_3, CH_2F_2 and CH_3F-based deposits prepared under different E_m (or F_d) conditions.

Table 5.1. Results of broad-scan XPS analyses of PP deposits on c-Si substrates obtained from DBD discharge plasmas in Ar/CH_xF_y mixtures (see text).

Sample	**C (at.%)**	**F (at.%)**	**O (at.%)**	**N (at.%)**	**Si (at.%)**
CHF_3 - 3 sccm ***	13.3 ± 0.8	44.8 ± 0.4	7.6 ± 0.6	18.2 ± 0.1	16.1 ± 1.0
CHF_3 - 3 sccm	51.9 ± 0.1	41.0 ± 0.1	3.2 ± 0.2	3.9 ± 0.2	ND
CHF_3 - 10 sccm	48.4 ± 0.5	48.1 ± 0.6	1.6 ± 0.1	1.9 ± 0.1	ND
CH_2F_2 - 2 sccm ***	14.5 ± 0.6	47.2 ± 0.6	2.4 ± 0.4	20.2 ± 0.3	15.7 ± 0.1
CH_2F_2 - 3 sccm	68.0 ± 0.6	19.5 ± 0.6	7.7 ± 0.4	4.8 ± 0.4	ND
CH_2F_2 - 4 sccm	66.3 ± 0.8	18.7 ± 0.4	9.4 ± 0.1	5.6 ± 0.3	ND
CH_2F_2 - 14 sccm	66.6 ± 0.1	28.0 ± 0.1	5.4 ± 0.1	ND	ND
CH_3F - 3 sccm	78.5 ± 0.1	12.5 ± 0.2	5.0 ± 0.3	4.0 ± 0.1	ND
CH_3F - 10 sccm	81.7 ± 0.1	11.1 ± 0.4	6.7 ± 0.3	0.5 ± 0.1	ND

*******: Ultra-thin coating (see text).

Considering CHF_3, the molecule discussed in this subsection, there existed strong competition between etching and deposition, depending on certain conditions in the DBD plasma zone (local gas composition and flow, for example). This accounts for the fact that at F_d = 3 sccm (i.e. below the 4 sccm transition), **Table 5.1** lists two sets of compositions, one corresponding to an ultra-thin deposit where etching tended to dominate. It is seen to have incorporated not only the expected C and F (beside H that is evidently not detected by XPS), but also Si (via atomic F-based etching of the Si wafer), N and O. Oxygen is nearly always present in PP coatings on account of reactions between trapped radicals and O_2 once the coating encounters air, a well-documented fact [39]. The presence of N, however, must be attributed to the earlier-mentioned likely presence of small air-leaks into the DBD reactor housing, in spite of the slight Ar overpressure.

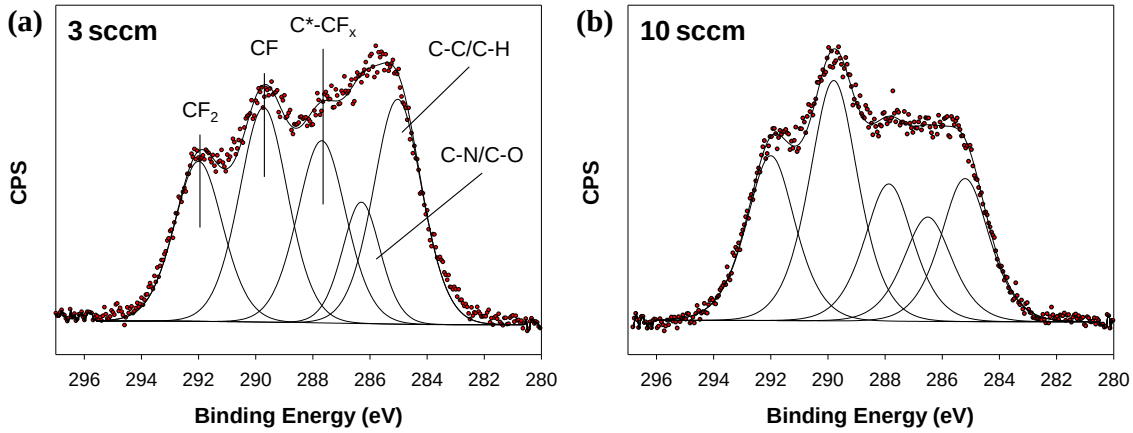

Figure 5.6. High-resolution (HR) C 1s XPS spectra of PP-CHF_3 coatings on c-Si substrates from mixtures with Ar, with (a) F_d = 3 sccm and (b) F_d = 10 sccm.

Figure 5.6 presents two high-resolution (HR) XPS spectra, (a) and (b), corresponding to F_d = 3 and 10 sccm deposits in **Table 5.1**, respectively. Both of these PP coatings were quite F-rich (41 and 48 at.%), but (a) showed a stronger C-C/C-H sub-peak in the deconvoluted HR XPS spectrum than (b). **Table 5.1** indicates F/C = 1 and 0.8 in (b) and (a), respectively, signaling substantial loss of F (from the initial precursor value F/C = 3) in both cases, but more at 3 sccm; this may have accounted for the above-discussed etching of Si, even though no Si was detected in either of the two PP coatings. It is interesting to point out the absence of a CF_3 contribution in the XPS spectra from possible CF_3 chain-end groups, unlike what was reported by Hubert *et al.* for the case of larger fluorocarbons (C_6F_{12}, C_6F_{14}) [75]. Under present conditions, "C_1" precursors apparently did not give rise to appreciable CF_3 chain-end concentrations, in spite of abundant CF_3 in the plasma, as revealed by OES. This observation is also noteworthy in regard to other sections below.

5.3.3.3 **Ar/CH_2F_2**

Figure 5.7 has three components, unlike the preceding CF_4 and CHF_3 counterparts: (a) is a log-log plot of E_m versus F_d for the case of Ar/CH_2F_2 mixtures in the range $0.9 \leq F_d \leq 40$ sccm; (b) represents J_m of the CF_2, CF_3, CH (386 nm) and CH (420 nm) bands, also on log-log scales; last, (c) presents deposition rate, r (in nm/minute), of PP coatings, all of (a-c) for the corresponding F_d values. Here are the main ensuing observations:

(i) In (a), as before, E_{m} decreased monotonically beyond $(E_{\mathrm{m}})_{max}$, that is, for F_{d} > 1.1 sccm; (b) showed a maximum in CF_2 at F_{d} = 1.1 sccm, followed by a drop, in accord with corresponding behaviors of the preceding F-richer molecules. However, unlike the case of CHF_3, the CF_3 band intensity decreased instead of rising, not illogical considering the high C-F bond strength: creating CF_3 from CH_2F_2 called for breakage of a C-F bond on another molecule in order to enable recombination; in **Fig. 5.5** we had noted that this was difficult beyond the 4 sccm transition. Here, we observed a somewhat similar "transition" at F_{d} ~ 4 sccm, but unlike that in CHF_3, CH bands were present even at low F_{d} values. This was no surprise in view of the additional H in this molecule, but both CH band intensities dropped sharply for F_{d} > 4 sccm.

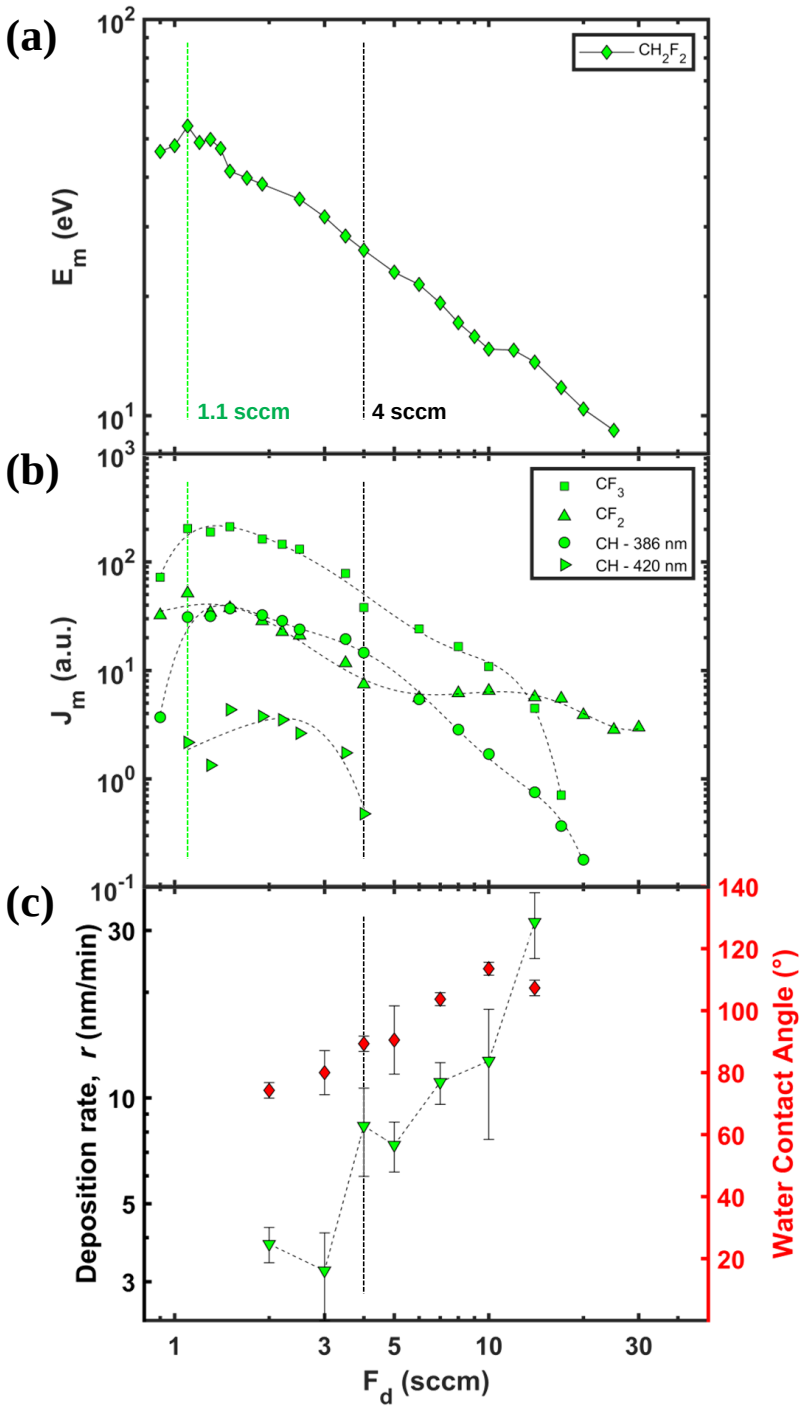

Figure 5.7. Plots of (a) E_m versus F_d; and (b) J_m versus F_d; (c) r (green) and water contact angle (red) versus F_d (see text for explanations), for the case of Ar/CH_2F_2 mixtures with $0.9 \leq F_d \leq 40$ sccm. Note log-log scales in (a) and (b).

(ii) Regarding the $r(F_d)$ plot in **Fig.5.7**(c), hardly any deposition occurred below the 4 sccm transition, again likely due to competition with etching reactions: In **Table 5.1** we noted that for F_d = 2 sccm an ultrathin deposit was obtained, one with very similar composition as for F_d = 3 sccm in the CHF_3 case. But for F_d > 4 sccm r was seen to have risen very markedly, to r > 30 nm/min at F_d = 14 sccm.

(iii) Also shown in part (c) of this figure (see red symbols and right-hand ordinate axis) are measurements of water contact angles (WCA) on the various coatings. We notice that WCA was directly related to F concentrations at the surfaces (see **Table 5.1**): the more "PTFE-like" the surface, the more hydrophobic was its character; for example, on smooth commercial Teflon® PTFE surfaces, WCA values have been reported to vary from 108° to 114° [79], close to that of the 10 sccm coating.

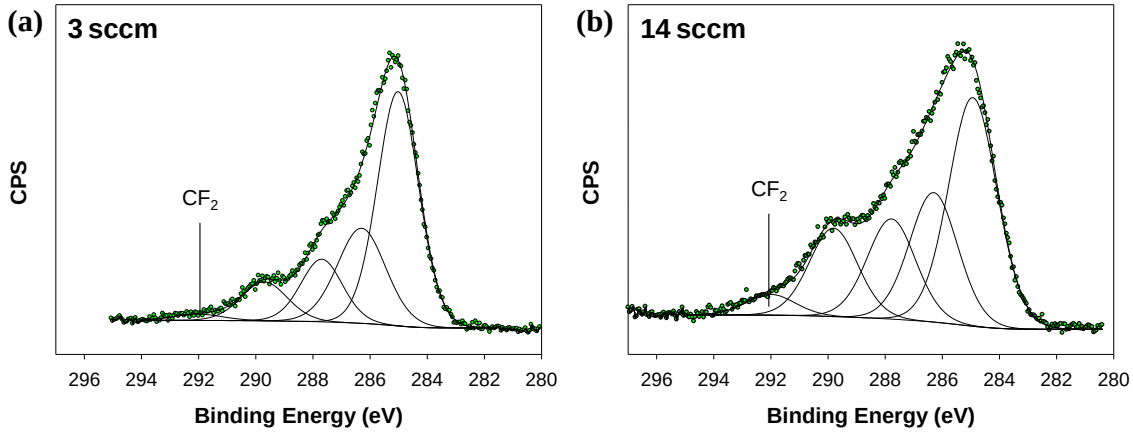

Figure 5.8. High-resolution (HR) C 1s XPS spectra of PP-CH_2F_2 coatings on c-Si substrates from mixtures with Ar, with (a) F_d = 3 sccm and (b) F_d = 14 sccm.

Coming back to PP film compositions (see **Table 5.1**), **Figure 5.8** presents HR C 1s XPS spectra for F_d = 3 and 14 sccm; they indicate only little presence of CF_2 groups, about 4% at 14 sccm but virtually none at 3 sccm, below the 4 sccm transition. Even though overall F content was appreciable (19 ≤ F ≤ 28 at.%), it was much lower than for CHF_3; the F/C ratios, 2 in the molecule, were respectively only 0.29 and 0.42 in the 3 sccm and 14 sccm PP deposits. As in the previous case, this bore witness to substantial molecular fragmentation and F-loss in the DBD plasma.

5.3.3.4 **Ar/CH_3F**

Figure 5.9 (a) is a log-log plot of E_m versus F_d for the case of Ar/CH_3F mixtures in the range $1 \leq F_d \leq 50$ sccm, while (b) again represents J_m of the CF_2, CF_3, CH (386 nm) and CH (420 nm) bands, also on log-log scales, for the corresponding F_d values. We can now make the following observations:

Logically, we note a reduced presence of F-bearing groups compared with **Figs. 5.5** and **5.7**, as expected from the F/C ratios of the respective precursors. Only in a rather limited regime above $(E_m)_{max}$ ($2 \leq F_d \leq 10$ sccm) could one observe measurable CF_3 and CF_2 band intensities, albeit much fainter than those of the CHF_3 and CH_2F_2 molecules. For the CF_3 case, in particular, that necessarily required *two additional* molecules to contribute their F atoms; logically, the high energies needed to satisfy such conditions occurred only in the vicinity of $(E_m)_{max}$, where precursor fragmentation was at its highest. It is noteworthy that the CH_3F molecule manifested the lowest $(E_m)_{max}$ value, even below that of CH_4 (see also **Fig. 5.2**), as well as the highest PP deposition rate, r. This latter aspect will be elaborated further in the Discussion (section 4).

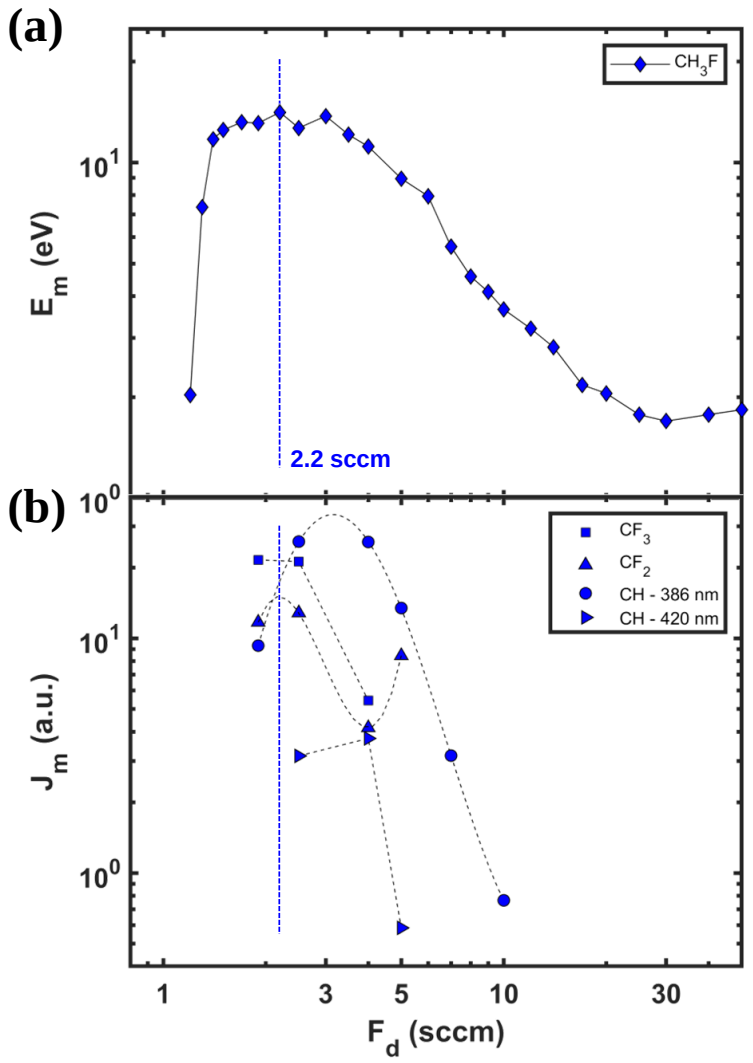

Figure 5.9. Plots of (a) E_m versus F_d; and (b) J_m versus F_d (see text for explanations), for the case of Ar/CH_3F mixtures with $1 \leq F_d \leq 50$ sccm (log-log scales, base 10).

Regarding PP film compositions (see **Table 5.1**), the following may be said: coatings at F_d = 3 and 10 sccm respectively contained only 12.5 and 11 at.% F; HR C 1s XPS spectra (not shown) revealed no CF_2 presence whatever, even at the higher F_d; by far the most prominent sub-peak was that due to C-C/C-H (i.e. hydrocarbon, at 285.0 eV binding energy). The coatings' F/C ratios were roughly 0.15, compared with 1 in the original molecule.

5.3.3.5 **Ar/CH_4**

Figure 5.10 (a) is a log-log plot of E_m versus F_d for the case of Ar/CH_4 (methane) mixtures in the range $2 \leq F_d \leq 50$ sccm, while (b) represents J_m of the two hydrocarbon bands, CH (386 nm) and CH (420 nm) for the corresponding F_d values. Here are the main observations:

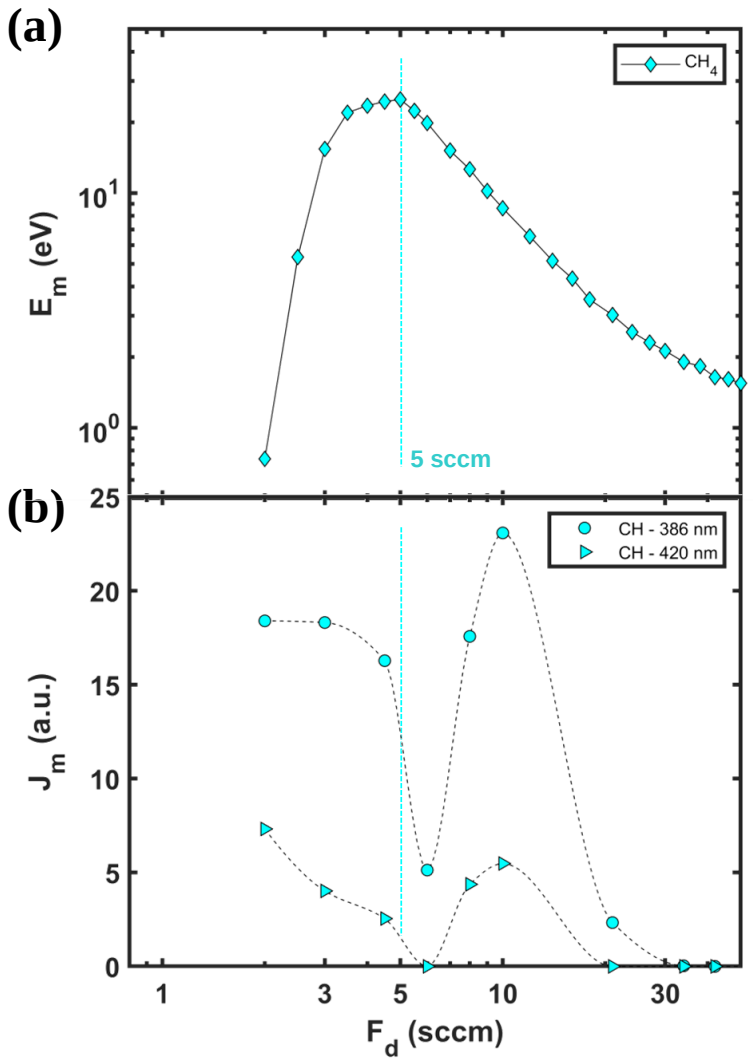

Figure 5.10. Plots of (a) E_m versus F_d (log-log scales, base 10); and (b) I_m versus F_d (see text for explanations), for the case of Ar/CH_4 mixtures with $2 \leq F_d \leq 50$ sccm.

For obvious reasons, absence of F in the molecule, CF_3 and CF_2 bands were not present. The CH band intensity, particularly that at 386 nm, was seen to be exceedingly sensitive to variation of E_m: beyond $(E_m)_{max}$, J_m dropped sharply, probably because the available energy was no

longer sufficient to abstract 3 H atoms from the CH_4 molecule. Particularly noteworthy and interesting were the abrupt dips in both CH band intensities, almost exactly at $(E_m)_{max}$, probably the result of near-total fragmentation of the methane molecule. Qualitatively identical $J_m(F_d)$ behaviors of the two CH bands for F_d > 5 sccm were compatible with the smoothly-decreasing E_m values in **Fig. 5.10**(a).

5.4 Discussion

This section is, first, devoted to an inspection and comparison of results obtained in preceding "Results" sub-sections pertaining to individual precursors.

In **Fig. 5.11** we have re-plotted the above-presented data for (a) CF_2, (b) CF_3 and (c) CH (386 nm) band intensities of the CH_xF_y precursors, using the same colors as before to help distinguish the individual compounds. At least two interesting observations can be made:

For (a), CF_2, nearly all precursor molecules displayed the same overall trend, namely that J_m dropped beyond $(E_m)_{max}$ of the respective E_m plots. The (red) CHF_3 curve displayed a maximum that was slightly higher and displaced toward lower F_d compared with the (black) CF_4 plot. This is logical if one considers the fact that it required less energy to form CF_2 by abstracting an (H + F) atom pair instead of two F atoms. The green CH_2F_2 plot, by the way, rather closely resembled the CHF_3 one; however, the blue CH_3F curve differed markedly in amplitude and shape, because here two molecules were necessarily involved.

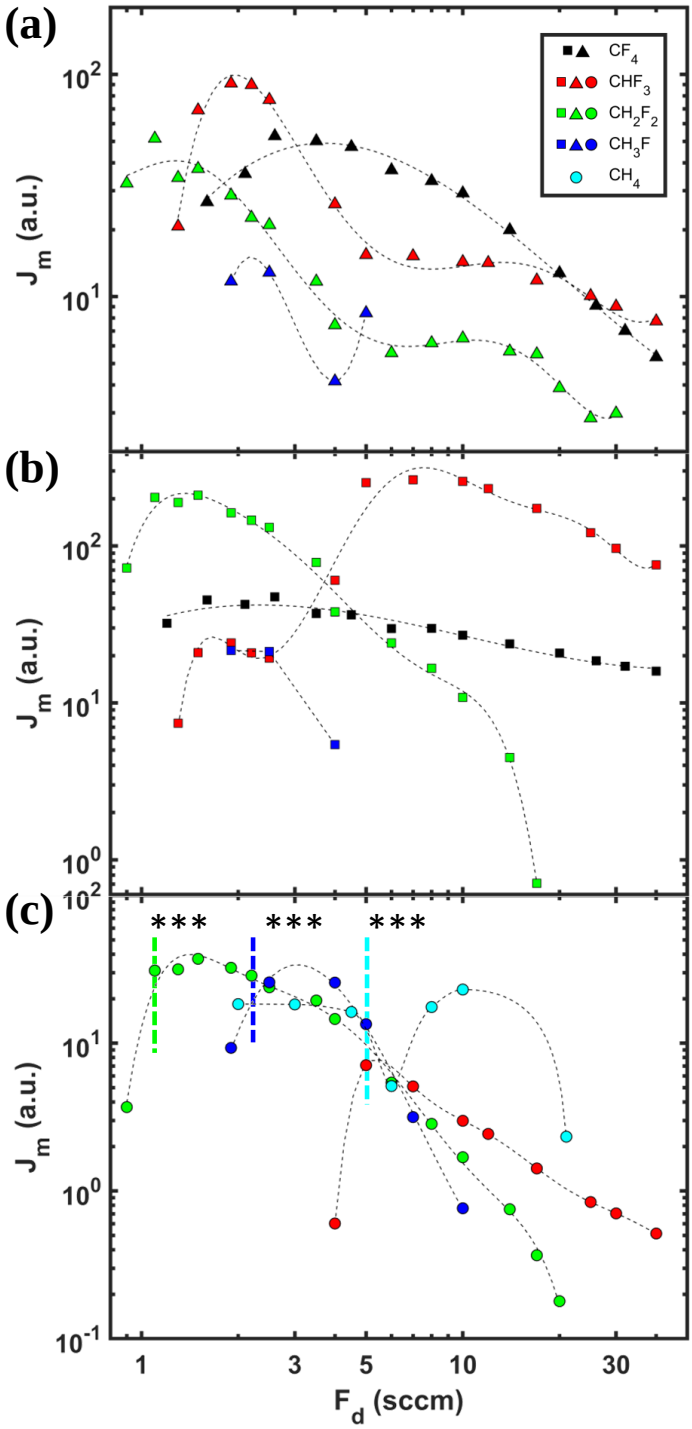

Figure 5.11. Log-log (base 10) plots of (a) CF_2, (b) CF_3, and (c) CH (386 nm) band intensities, J_m, versus F_d of the CH_xF_y molecules, using the same colors as previously.

In (b), the most striking difference in CF_3 plots was the *opposite* trends noted between the (red) CHF_3 curve and the green one for CH_2F_2: The former rose markedly *after* the earlier-discussed transition (F_d ~ 4 sccm), pointing to more favorable CF_3 formation at higher F_d (lower E_m) via C-H bond breakage. On the other hand, in the case of CH_2F_2, it was necessary to abstract *two* hydrogens and to recruit an F atom on a nearby molecule. Clearly, that became less and less likely with rising F_d (decreasing E_m); that statement applied even more strongly to the blue (CH_3F) curve, in which case no less than *three* molecules were required to form CF_3.

In (c), the three vertical lines identify positions of $(E_m)_{max}$ for three of the molecules involved. It is interesting to note that the maximum intensity, J_m, of the CH band was always encountered somewhat to the right of $(E_m)_{max}$. A plausible reason may be that, to the left, there was too much energy (not enough precursor molecules), leading to excessive (possibly *total*) fragmentation.

Figure 5.12 represents measurements of PP deposition rates, r (in nm/min) for (a) F_d = 3 sccm and (b) F_d = 10 sccm, corresponding to the indicated molecules (note that the "etchant", CF_4, is included but never led to any measurable deposition). The dotted bar in (a) for the case of CHF_3 symbolizes the earlier-discussed fact that under these experimental conditions, this precursor yielded very non-uniform deposits (see **Table 5.1**); they were of either ultrathin (near-zero) thickness, or of that corresponding to the maximum bar-height, ca. 3 nm/min, obviously due to the competition between etching and deposition. Also shown in parts (a) and (b) of this figure (see red symbols and right-hand ordinate axes) are measurements of water contact angles (WCA) on the various coatings. In some cases, one may note *two* values, a lower and an upper one. The former represents ultrathin coatings in **Table 5.1** resulting from etch/deposition competition, so of little interest here.

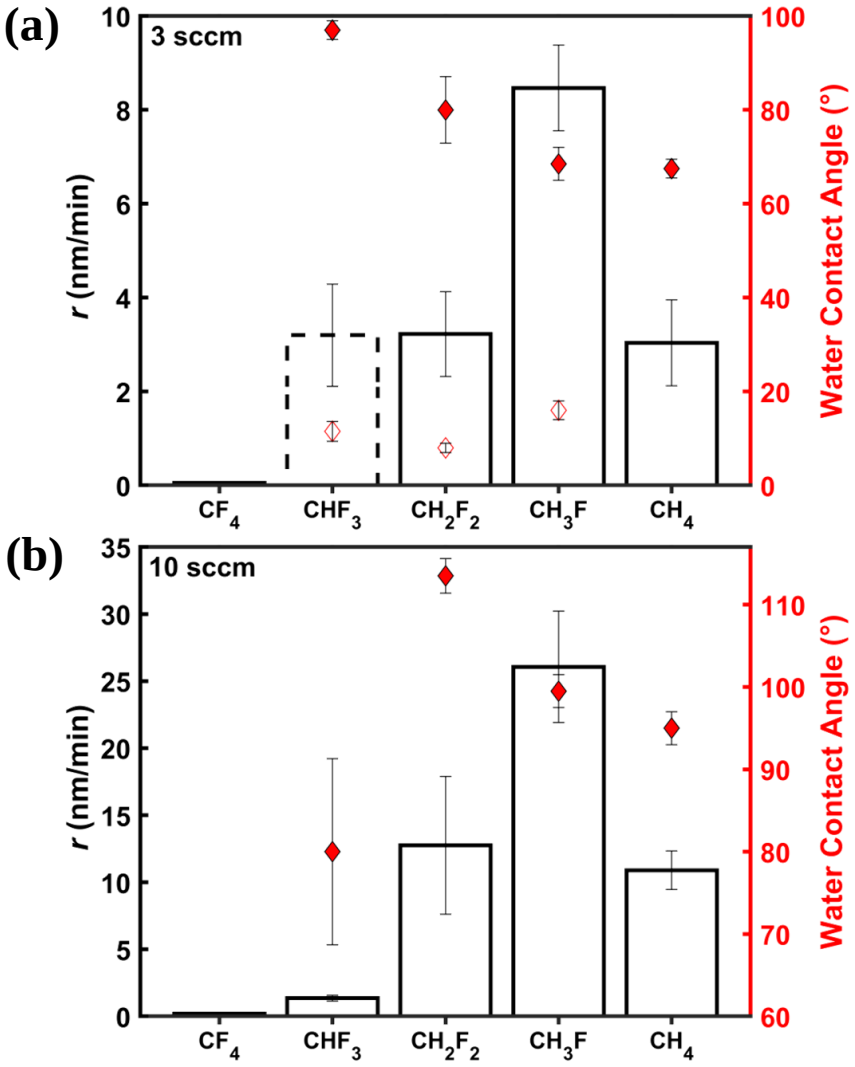

Figure 5.12. Deposition rates, r (in nm/min) of PP coatings from the CH_xF_y molecules, for (a) F_d = 3 sccm and (b) F_d = 10 sccm. The colored data points represent contact angles of sessile water droplets on the corresponding PP surfaces.

Inspecting the upper (higher) values, however, we again notice, as before in connection with **Fig. 5.7**(c), that WCA was directly related to F concentrations at the surfaces (see **Table 5.1**). The value ca. 114º, close to that of Teflon® PTFE, had already been pointed out on **Fig. 5.7**(c) [79]. Therefore, like the preceding authors,[68-73] we have developed a method for depositing very hydrophobic coatings under conditions that are potentially amenable to commercial exploitation

at relatively low cost. On a nanorough surface, the coating's WCA value could even become *superhydrophobic*, with an enhanced WCA, virtually near 180°.[80]

Regarding the other data portrayed in (a) and (b), regardless of F_d, CH_4 was seen to have lower r values than CH_3F, the precursor with by far the highest ones; as pointed out earlier (section 3.3.4), the latter was mostly "hydrocarbon-like", with only ca. 11 to 12 at.% F. This completely unexpected high r value remains puzzling at present, but it must have a rational thermodynamic/energy-related explanation in terms of C-H and C-F bond energies in that molecule, their fragmentation in the DBD plasma and the formation of other volatile species (H_2, F_2, HF, …). In **Table 5.2** we list r values, along with initial slopes, [d(E_m)/d(F_d)], of the individual precursors' E_m versus 1/F_d plots in **Fig. 5.2**. As the F/C ratio increased, so did the slope, the exception once again being CH_3F: this molecule had a two-fold higher deposition rate, r.

The topics discussed above are now the object of further investigation, along with similar studies involving higher molecular weight fluoro- and other halocarbons.

Table 5.2. Compilation of calculated E_m (1/F_d) slopes, deposition rates, *r*, and $(E_m)_{max}$ values for DBD plasmas in Ar/CH_xF_y mixtures (see text).

Molecule	**Slope (W)**	**Deposition rate, *r*, at 10 sccm (nm/min)**	**$(E_m)_{(max)}$ (eV)**
CF_4	11.9	N/A	53.2
CHF_3	10.0	1.3 ± 0.2	38.9
CH_2F_2	8.7	13 ± 5	53.8
CH_3F	2.2	26 ± 4	14.1
CH_4	2.7	11 ± 1	25.0

5.5 Conclusions

The method we have developed for fundamentally understanding energetic exchanges between (precursor) molecules and Ar carrier gas atoms in dielectric barrier discharge (DBD) plasmas has now been extended to the family of five hydrofluoromethanes, CH_xF_y. These precursors, typically in ‰ concentration, were mixed with 10 slm of Ar in a 20 kHz, 8 kV (peak-to-peak) DBD corresponding to an average energy per cycle of 1600 μJ for the case of pure Ar in the large (216 cm^2) DBD reactor [76]. Even in the case of these highly electronegative F-containing additive gases, which tend to display filamentary discharge behavior, time-averaged electrical measurements nevertheless yielded reliable, reproducible values of E_m, the energy absorbed per molecule. For each of the investigated compounds, E_m and optical emission spectroscopic (OES) "intensities per molecule", J_m, of selected bands, namely CF_2, CF_3, and two CH emissions at 386 and 420 nm wavelengths, were plotted as a function of precursor flow rate, F_d. These measurements turned out to be remarkably revealing as diagnostics of the plasmas' physico-chemistry, in that they provided much valuable information about molecular fragmentation as a function of E_m (or F_d).

The influence of the precursors' chemical structures and fragmentation behaviors under varying plasma conditions was also investigated by examining thin deposited plasma polymer (PP) coatings, whenever these formed under competing etching/deposition reactions: as anticipated, the strongly etching CF_4 molecule never led to deposition under any circumstances. In addition to measuring PP deposition rates, r, and water contact angles, we also investigated their relationships with E_m values and fluorine (F) concentrations determined from XPS measurements. A very unexpected result, namely that CH_3F precursor displayed the highest r value, significantly exceeding even that of CH_4, is now being further investigated.

Acknowledgments: The authors are grateful for financial support from the Natural Sciences and Engineering Research Council of Canada (NSERC) and from the *Fonds de recherche du Québec – Nature et technologies* (FRQNT). We thank Yves Leblanc for skilled technical support.

CHAPTER 6 GENERAL DISCUSSION

The field of "cold" plasma science and technology, for many years focused on the use of LP, h.f. (r.f.- or microwave-powered) discharges, has over recent decades evolved towards ones at AP, generally fed by mid-frequency power (several tens of kHz). Among the latter types of plasmas one may list DBD and plasma jets as the two most prominent implementations for technological use; numerous commercial vendors world-wide now offer hardware based on these.

In this M.Sc.A. thesis, we deal exclusively with DBD plasmas; in spite of a vast prior literature (see references in **Chapters 1** and **2**, for example), we can truthfully state that several important breakthroughs have been made in the course of this work; here are the main ones:

1) By building and carefully characterizing two DBD reactors of vastly different geometries (areas, A = 5.1 and 216 cm^2), we somewhat fortuitously discovered that non-filamentary, "APGD"-like behavior appears to be the norm in large-area reactor geometries when using Ar carrier gas (especially with small concentrations of added molecular "dopant" gases or vapors). This important discovery is in stark contrast with teachings from the literature [25] which list only ketones and ammonia as "dopant" additives possessing this capability.
2) We have greatly expanded use of the powerful methodology developed in this laboratory for measuring the electrical energy, E_g, dissipated per discharge cycle of the applied a.c. voltage, V_a. This was accomplished by comparing the characteristics of pure noble gas (He, Ar, mostly) DBDs in the small and large-area reactors (see **Chapter 4**), along with data from the literature. The reliability of this methodology, which can replace well-established, but potentially problematic, techniques such as Lissajous figures, could be absolutely and objectively established, for example by breakdown field measurements (and by calorimetry, in an earlier paper [8]).
3) Using only the large (pilot-scale) reactor with Ar carrier gas and judiciously-selected electrical operating conditions (f = 20 kHz; V_a = 8 kV_{p-p}), we conducted an original study on a "new" family of organic precursor gases, namely *hydrofluoromethanes* (CH_xF_y, $0 \leq x \leq 4$; $y = 4 - x$). In spite of the extreme electronegativity of fluorocarbon compounds like these, the above-mentioned (see item 1), which led to more filamentary discharges, the

time-averaged traces of I_d were smooth enough to permit reliable measurements of E_m, the energy per molecule (in eV) absorbed from the plasma, as meaningfully as in earlier articles from this laboratory. Indeed, this new contribution (**Chapter 5**) constitutes the text of a manuscript that has been published in *Plasma Processes and Polymers* as number 8 in a series of such articles related to different organic precursor compounds, mostly for deposition of plasma polymer (PP) coatings. The present set of CH_xF_y-based PP films have been characterized by XPS and CAG measurements.

4) In **Chapter 5** we also reported plasma-diagnostic experiments based on optical emission spectroscopy (OES), which for the case of the CH_xF_y family lent itself to an original semi-quantitative study that was found to mesh remarkably well with the other measurements mentioned under item 3) above.
5) Finally, in **Appendix A**, we present an article, published in 2015 (prior to commencing this M.Sc.A.), of which the author of this thesis was also lead author. This paper, in the prestigious journal *Langmuir*, in turn, presents results pertaining to a family of three organic acids, but also a classification scheme based on measurements of $E_{m(max)}$, the maximum value of E_m in its plot versus M, the molar mass of the molecules. This type of classification / summary holds much promise for future in-depth studies related to our methodology (see also next chapter, Conclusions).

In summary, this research contributes several new insights, for example those listed above, into the physics and technology of dielectric barrier discharges, a field that is presently experiencing enormous growth in pure and applied plasma science and technology.

CHAPTER 7 CONCLUSION AND RECOMMENDATIONS

This M.Sc.A. thesis is quite "unusual" in that it contains a sizeable body of original research results in the form of published articles (**Chapters 4, 5** and **Appendix A**), all in international, peer-reviewed journals. Indeed, this thesis is part of a long-duration program on dielectric barrier discharge (DBD) plasmas that can be said to have commenced in the 1980s and that will foreseeably continue well into the future.

The circumstances described above can simply be explained by the fact that "cold" DBD plasmas are of very great scientific and technological interest, wherein the latter extends over many diverse fields. Those include, for example, surface modification of polymers for adhesion enhancement, plasma-enhanced chemical vapor deposition (PECVD) of thin coatings, and more recently plasma medicine, a very rapidly expanding multi-disciplinary topic involving not only physicists and chemists, but also biologists and clinicians. The reader may consult the review article by U. Kogelschatz [18] for a more complete list of applications, but also for the underlying fundamental science: even though that paper is now 16 years old, it remains one of the most-cited references and introductions for newcomers to this field.

As mentioned in the preceding chapter (**Chapter 6**, General Discussion), the work presented here includes several important breakthroughs; they will not be repeated, but each of them can readily constitute the starting point for fruitful extension. The next section presents some suggestions for further work.

7.1 Recommendations for future work

The fact that even the most *electronegative* additives to Ar-based DBD (the fluorocarbons we have investigated in **Chapter 5**) do not appear to significantly perturb quantifying the key parameters V_{gap} and I_{d} that give access to E_{g} via equation 4.15 signifies that the methodology we developed for evaluating E_{m} can now without doubt be extended to virtually all remaining families of (volatile) precursor compounds. These should include other halocarbons based on Cl or mixed F + Cl chemistries.

(a) From a more "electrical engineering" point of view, this measurement technique can be explored as a replacement for the "Lissajous figures" method going back to the 1940s,

which has revealed itself to entail serious pitfalls, even in circumstances (unlike here) where no "plasma-chemical" reactions are involved.

(b) The "large" pilot-scale reactor reported in **Chapters 4** and **5** has revealed itself to be very versatile, but this does not preclude the possibility of still further improvements. These could include:

- Even larger electrode area (A > 216 cm^2);
- A gas diffuser that assures optimum uniformity of deposits over the entire width of the discharge zone;
- An improved mounting of the (parallel) electrode assemblies;
- Gas metering capabilities over greater ranges than currently accessible; this could include:
- Improved thermal uniformity to avoid possible undesired condensation of precursor molecules with higher molecular weight / lower vapor pressure;
- Improvements to current power supply (better impedance matching), and possible improvements of the MATLAB code.

7.2 Contributions by the Author, Sean Watson (S.W.)

As mentioned above, S.W. joined Wertheimer's laboratory while still an undergraduate in 2014, and he has been working as lead-author of the team comprising authors of articles presented in Chapters 4, 5 and Appendix A. He has worked completely autonomously, for example, in gathering and reducing data for ΔE_g and E_m determinations, not only in those three articles, but also in others listed in Appendix B. In Chapter 5, he alone developed and executed the methodology used for OES measurements and their interpretation. It is not considered necessary to present further details of S.W.'s multiple contributions to this ongoing research program.

REFERENCES

[1] B. Nisol. Atmospheric pressure plasma synthesis of biocompatible poly(ethylene glycol)-like coatings. Ph.D. thesis, Université libre de Bruxelles, Brussels, 2011.

[2] D. Pappas, *J. Vac. Sci. Technol. A* **2011,** *29,* 020801 (17 pp.).

[3] M. Gamez-Garcia. Study of XLPE degradation by the action of partial discharges. Ph.D. thesis, École Polytechnique, Montréal, Québec, 1985.

[4] C. Hudon. Étude de dégradation des résines époxy sous l'action des décharges partielles. Ph.D. thesis, École Polytechnique, Montréal, Québec, 1993.

[5] R. Bartnikas, *J. Appl. Phys.* **1969,** *40,* 1974.

[6] S. F. Miralaï, E. Monette, R. Bartnikas, G. Czeremuszkin, M. Latrèche, M. R. Wertheimer, *Plasmas and Polym.* **2000,** *5,* 63.

[7] I. Radu, R. Bartnikas, M. R. Wertheimer, *IEEE Trans. Plasma Sci.* **2003,** *31,* 1363.

[8] M. Archambault-Caron, H. Gagnon, B. Nisol, K. Piyakis, M. R. Wertheimer, *Plasma Sources Sci. Technol.* **2015,** *24,* 045004 (16 pp).

[9] B. Nisol, H. Gagnon, S. Lerouge, M. R. Wertheimer, *Plasma Process. Polym.* **2016,** *13,* 366.

[10] P. Decomps, F. Massines, C. Mayoux, *Acta Phys. Univ. Comen.* **1994,** *35,* 47.

[11] G. Nersisyan, W. G. Graham, *Plasma Sources Sci. Technol.* **2004,** *13,* 582.

[12] S. Hofmann, A. F. H. v. Gessel, T. Verreycken, P. Bruggeman, *Plasma Sources Sci. Technol.* **2011,** *20,* 065010 (12 pp).

[13] R. Tyata, D. Subedi, R. Shrestha, C. Wong, *Pramana - J. Phys.* **2013,** *80,* 507.

[14] N. Merbahi, N. Sewraj, F. Marchal, Y. Salamero, P. Millet, *J. Phys. D: Appl. Phys.* **2004,** *37,* 1664.

[15] B. Nisol, S. Watson, S. Lerouge, M. R. Wertheimer, *Plasma Process. Polym.* **2016,** *13,* 557.

[16] S. Watson, B. Nisol, S. Lerouge, M. R. Wertheimer, *Langmuir* **2015,** *31,* 10125.

[17] B. Nisol, S. Watson, S. Lerouge, M. R. Wertheimer, *Plasma Process. Polym.* **2016,** *13,* 900.

[18] U. Kogelschatz, *Plasma Chem. Plasma Process.* **2003,** *23,* 1.

[19] P. Kurunczi, J. Lopez, H. Shah, K. Becker, *Int. J. Mass Spectrom.* **2001,** *205,* 277.

[20] V. Tarasenko, *Pure Appl. Chem.* **2009,** *74,* 465.

[21] K. H. Becker, P. F. Kurunczi, M. Moselhy, K. H. Schoenbach, *Proc. SPIE* **2002,** *4460,* 239.

[22] A. Morozov, T. Heindl, R. Krücken, A. Ulrich, J. Wieser, *J. Appl. Phys.* **2008,** *103,* 103301 (8 pp).

[23] S. Kanazawa, M. Kogoma, T. Moriwaki, S. Okazaki, *J. Phys. D: Appl. Phys.* **1988,** *21,* 838.

[24] F. Massines, A. Rabehi, P. Decomps, R. B. Gadri, P. Ségur, C. Mayoux, *J. Appl. Phys.* **1998,** *83,* 2950.

[25] F. Massines, C. Sarra-Bournet, F. Fanelli, N. Naudé, N. Gherardi, *Plasma Process. Polym.* **2012,** *9,* 1041.

[26] F. Massines, N. Gherardi, N. Naudé, P. Ségur, *Eur. Phys. J. - Appl. Phys.* **2009,** *47,* 22805 (10 pp).

[27] I. Radu, R. Bartnikas, G. Czeremuszkin, M. R. Wertheimer, *IEEE Trans. Plasma Sci.* **2003,** *31,* 411.

[28] N. Gherardi, G. Gouda, E. Gat, A. Ricard, F. Massines, *Plasma Sources Sci. Technol.* **2000,** *9,* 340.

[29] I. Enache, N. Naudé, J. P. Cambronne, N. Gherardi, F. Massines, *Eur. Phys. J. - Appl. Phys.* **2006,** *33,* 15.

[30] D. Merche, N. Vandencasteele, F. Reniers, *Thin Solid Films* **2012,** *520,* 4219.

[31] G. Fridman, G. Friedman, A. Gutsol, A. B. Shekhter, V. N. Vasilets, A. Fridman, *Plasma Process. Polym.* **2008,** *5,* 503.

[32] M. R. Wertheimer, M. Ahlawat, B. Saoudi, R. Kashyap, *Appl. Phys. Lett.* **2012,** *100,* 201112 (4 pp).

[33] A. Berchtikou, J. Lavoie, V. Poenariu, B. Saoudi, R. Kashyap, M. R. Wertheimer, *IEEE Trans. Dielectr. Electr. Insul.* **2011,** *18,* 24.

[34] S. Okazaki, M. Kogoma, M. Uehara, Y. Kimura, *J. Phys. D: Appl. Phys.* **1993,** *26,* 889.

[35] A. V. Pipa, T. Hoder, J. Koskulics, M. Schmidt, R. Brandenburg, *Rev. Sci. Instrum.* **2012,** *83,* 075111 (10 pp).

[36] R. Morent, N. De Geyter, T. Jacobs, S. Van Vlierberghe, P. Dubruel, C. Leys, E. Schacht, *Plasma Process. Polym.* **2009,** *6,* S537.

[37] T. C. Manley, *Trans. Electrochem. Soc.* **1943,** *84,* 83.

[38] J. Goodman, *J. Polym. Sci.* **1960,** *44,* 551.

[39] *Plasma Polymerization*, H. K. Yasuda, Academic Press Inc, Orlando FL, **1985**.

[40] *Plasma Polymerization Processes*, H. Biederman, Y. Osada, Elsevier, Amsterdam, **1992**.

[41] R. Thyen, A. Weber, C.-P. Klages, *Surf. Coat. Technol.* **1997,** *97,* 426.

[42] O. Goossens, E. Dekempeneer, D. Vangeneugden, R. Van de Leest, C. Leys, *Surf. Coat. Technol.* **2001,** *142–144,* 474.

[43] P. Heyse, R. Dams, S. Paulussen, K. Houthoofd, K. Janssen, P. A. Jacobs, B. F. Sels, *Plasma Process. Polym.* **2007,** *4,* 145.

[44] P.-L. Girard-Lauriault, P. Desjardins, W. E. S. Unger, A. Lippitz, M. R. Wertheimer, *Plasma Process. Polym.* **2008,** *5,* 631.

[45] N. De Geyter, R. Morent, S. Van Vlierberghe, P. Dubruel, C. Leys, L. Gengembre, E. Schacht, E. Payen, *Prog. Org. Coat.* **2009,** *64,* 230.

[46] J. Petersen, R. Bechara, J. Bardon, T. Fouquet, F. Ziarelli, L. Daheron, V. Ball, V. Toniazzo, M. Michel, A. Dinia, D. Ruch, *Plasma Process. Polym.* **2011,** *8,* 895.

[47] A. Kakaroglou, G. Scheltjens, B. Nisol, I. De Graeve, G. Van Assche, B. Van Mele, R. Willem, M. Biesemans, F. Reniers, H. Terryn, *Plasma Process. Polym.* **2012,** *9,* 799.

[48] R. d'Agostino, P. Favia, R. Förch, C. Oehr, M. R. Wertheimer, *Plasma Process. Polym.* **2010,** *7,* 363.

[49] D. Hegemann, M. M. Hossain, E. Körner, D. J. Balazs, *Plasma Process. Polym.* **2007,** *4,* 229.

[50] D. Hegemann, E. Körner, S. Guimond, *Plasma Process. Polym.* **2009,** *6,* 246.

[51] D. Hegemann, *J. Phys. D: Appl. Phys.* **2013,** *46,* 205204 (8 pp).

[52] H. Becker, in *Wissenschaftliche Veröffentlichungen aus dem Siemens-Konzern 7*, Springer-Verlag, Berlin **1920**, p. 76.

[53] H. K. Yasuda, T. Hirotsu, *J. Polym. Sci., Polym. Chem. Ed.* **1978,** *16,* 743.

[54] A. Kakaroglou, B. Nisol, K. Baert, I. De Graeve, F. Reniers, G. Van Assche, H. Terryn, *Roy. Soc. Chem. Adv.* **2015,** *5,* 27449.

[55] H. Gagnon, K. Piyakis, M. R. Wertheimer, *Plasma Process. Polym.* **2014,** *11,* 106.

[56] B. Nisol, S. Watson, S. Lerouge, M. R. Wertheimer, *Plasma Process. Polym.* **2017,** *14,* 1600191.

[57] L. G. Christophorou, J. K. Olthoff, *Gaseous Dielectrics VIII*. Kluwer-Plenum: New York, 1998.

[58] E. E. Kunhardt, W. W. Byszewski, *Phys. Rev. A* **1980,** *21,* 2069.

[59] L. Babich, T. V. Loĭko, *IEEE Trans. Plasma Sci.* **2016,** *44,* 3243.

[60] *Atmospheric Pressure Plasma Treatment of Polymers: Relevance to Adhesion*, M. Thomas, K. L. Mittal, (Eds.), John Wiley and Sons/Scrivener Publishing, Hoboken/Salem, **2013**.

[61] J. Mertens, S. Watson, B. Nisol, M. R. Wertheimer, F. Reniers, *Plasma Process. Polym.* **2019,** *16,* 1800186.

[62] D. Hegemann, B. Nisol, S. Watson, M. R. Wertheimer, *Plasma Process. Polym.* **2016,** *13,* 834.

[63] D. Hegemann, B. Nisol, S. Watson, M. R. Wertheimer, *Plasma Chem. Plasma Process.* **2017,** *37,* 257.

[64] D. Hegemann, B. Nisol, S. Gaiser, S. Watson, M. R. Wertheimer, *Phys. Chem. Chem. Phys.* **2019,** *21,* 8698.

[65] D. Loffhagen, M. M. Becker, A. K. Czerny, J. Philipp, C.-P. Klages, *Contrib. Plasma Phys.* **2018,** *58,* 337.

[66] R. d'Agostino, F. Cramarossa, F. Fracassi, F. Illuzzi, "2 - Plasma Polymerization of Fluorocarbons", in *Plasma Deposition, Treatment, and Etching of Polymers*, R. d'Agostino, Ed. Academic Press, San Diego **1990**, p. 95.

[67] A. Vogelsang, A. Ohl, R. Foest, K.-D. Weltmann, *Plasma Process. Polym.* **2013,** *10,* 364.

[68] I. Vinogradov, A. Lunk, *Plasma Process. Polym.* **2005,** *2,* 201.

[69] F. Fanelli, F. Fracassi, R. d'Agostino, *Plasma Process. Polym.* **2007,** *4,* S430.

[70] F. Fanelli, G. Di Renzo, F. Fracassi, R. d'Agostino, *Plasma Process. Polym.* **2009,** *6,* S503.

[71] F. Fanelli, *Plasma Process. Polym.* **2009,** *6,* 547.

[72] E. Abadjieva, A. E. D. M. van der Heijden, Y. L. M. Creyghton, J. R. van Ommen, *Plasma Process. Polym.* **2012,** *9,* 217.

[73] J. Mertens, J. Hubert, N. Vandencasteele, M. Raes, H. Terryn, F. Reniers, *Surf. Coat. Technol.* **2017,** *315,* 274.

[74] B. Nisol, F. Reniers, *J. Electron Spectrosc. Relat. Phenom.* **2015,** *200,* 311.

[75] J. Hubert, N. Vandencasteele, J. Mertens, P. Viville, T. Dufour, C. Barroo, T. Visart de Bocarmé, R. Lazzaroni, F. Reniers, *Plasma Process. Polym.* **2015,** *12,* 1174.

[76] S. Watson, B. Nisol, H. Gagnon, M. Archambault-Caron, F. Sirois, M. R. Wertheimer, *IEEE Trans. Plasma Sci.* **2019,** *47,* 2680.

[77] B. A. Cruden, K. K. Gleason, H. H. Sawin, *J. Appl. Phys.* **2002,** *91,* 9547.

[78] *The Identification of Molecular Spectra, 3rd edition.*, R. W. B. Pearse, A. G. Gaydon, Chapman and Hall, London, **1963**.

[79] M. K. Bernett, W. A. Zisman, *J. Phys. Chem.* **1959,** *63,* 1241.

[80] S. Wang, L. Jiang, *Adv. Mater.* **2007,** *19,* 3423.

[81] *Low Temperature Plasmas: Fundamentals, Technologies, Techniques*, R. Hippler, H. Kersten, M. Schmidt, K. H. Schoenbach, (Eds.), Wiley-VCH, Berlin, **2008**.

[82] G. Øye, V. Roucoules, A. M. Cameron, L. J. Oates, N. R. Cameron, P. G. Steel, J. P. S. Badyal, B. G. Davis, D. Coe, R. Cox, *Langmuir* **2002,** *18,* 8996.

[83] D. B. Haddow, R. M. France, R. D. Short, J. W. Bradley, D. Barton, *Langmuir* **2000,** *16,* 5654.

[84] K. S. Siow, L. Britcher, S. Kumar, H. J. Griesser, *Plasma Process. Polym.* **2006,** *3,* 392.

[85] E. E. Johnston, J. D. Bryers, B. D. Ratner, *Langmuir* **2005,** *21,* 870.

[86] B. W. Muir, A. Tarasova, T. R. Gengenbach, D. J. Menzies, L. Meagher, F. Rovere, A. Fairbrother, K. M. McLean, P. G. Hartley, *Langmuir* **2008,** *24,* 3828.

[87] A. Michelmore, P. Gross-Kosche, S. A. Al-Bataineh, J. D. Whittle, R. D. Short, *Langmuir* **2013,** *29,* 2595.

[88] B. Nisol, G. Oldenhove, N. Preyat, D. Monteyne, M. Moser, D. Perez-Morga, F. Reniers, *Surf. Coat. Technol.* **2014,** *252,* 126.

[89] *Industrial Plasma Technology: Applications from Environmental to Energy Technologies*, Y. Kawai, H. Ikegami, N. Sato, A. Matsuda, K. Uchino, M. Kuzuya, A. Mizuno , (Eds.), Wiley-VCH Verlag GmbH & Co. KGaA, Weinheim, **2010**.

[90] *Coatings for Biomedical Applications*, M. Driver, (Ed.), Woodhead Publishing, Cambridge, **2012**.

[91] H. Savoji, A. Hadjizadeh, M. Maire, A. Ajji, M. R. Wertheimer, S. Lerouge, *Macromol. Biosci.* **2014,** *14,* 1084.

APPENDIX A ARTICLE 3: ENERGETICS OF MOLECULAR EXCITATION, FRAGMENTATION AND POLYMERIZATION IN A DIELECTRIC BARRIER DISCHARGE WITH ARGON CARRIER GAS

Article published in ***Langmuir* 2015, 31, pp. 10125−10129**

Sean Watson, Bernard Nisol, Sophie Lerouge, Michael Robert Wertheimer

Abstract—We report experiments at atmospheric pressure (AP) using a dielectric barrier discharge (DBD) reactor designed for plasma polymerization (PP) with "monomers" at ‰ concentrations in ca. 10 standard liters per minute of argon (Ar) carrier gas. We have perfected a method for measuring E_g, the energy dissipated per cycle of the applied a.c. high voltage, $V_a(f)$, but the focus here is on ΔE_g, the energy difference with and without a flow, F_d, of monomer in the Ar flow, the plasma being sustained at $V_a(f)$ = 2.8 kV_{rms}, f = 20 kHz. From ΔE_g and F_d, we derive a characteristic energy per molecule, E_m (in eV), and investigate plots of E_m versus F_d and $1/F_d$ for three model "monomers": formic, acetic and acrylic acid. These data, along with those for lighter or heavier organic compounds, reveal novel information about energy absorption from the plasma and ensuing polymerization reactions.

A.1 Introduction

Plasma processing science and technology (PPST) has grown enormously since its humble beginnings in the 1950s and 60s. A leading sub-field of PPST is plasma-enhanced chemical vapor deposition (PECVD), the fabrication of thin film deposits on solid substrates near ambient temperature [81]. In cases where the precursor gas or vapor is an organic compound, one speaks of plasma polymerization; the resulting plasma-polymer (PP) deposits have certain features in common with conventional polymeric solids, but they are fundamentally different in most respects: Their structure is amorphous, highly cross-linked, and their composition depends intimately on the particular set of selected plasma-deposition parameters [39, 81]. Major advantages of PP coatings are to enable surface modification of any solid substrate without affecting its bulk properties, and to tailor surface chemistry and -energy by creating polar chemical moieties (e.g. amines [82], carboxylic or other functional groups [83, 84]) that can govern solid-liquid interfacial interactions. This can help immobilize biomolecules or living cells [84] or, on the other extreme, create anti-fouling surfaces that *inhibit* adhesion of proteins and harmful cells like bacteria [85-88]. Of course, there exist numerous other applications for PP deposits, but we shall restrict this discussion to biomedical science and technology. For example, PP-polyethylene glycol (PEG-like) coatings are known for their powerful antifouling characteristics, attributed to strong interaction with water molecules. However, retention of the responsible ether groups requires near-perfect control of plasma chemistry, generally achieved by using mild (low-power) activation of the precursor molecules [85-88]. This is merely one example, where strict control of fabrication conditions dramatically affects successful outcome.

Like most other PPST procedures, PECVD and PP were almost exclusively carried out under partial vacuum during the first few decades, but this has changed since roughly twenty years. AP plasma processing has gained much interest because the absence of a costly vacuum installation promises easier, more economical implementation [25]. DBD constitute the main approach that enables scale-up for industrial processing [18]; DBD plasmas may be obtained in gaps between two electrode surfaces at least one of which is covered by a dielectric. They, too, are non-equilibrium (cold) plasmas, useful in numerous plasma-chemical reactions beside PECVD and PP, such as ozone synthesis, surface modification of polymers, abatement of pollutants, excimer lamps, and others [18]. Even though the primary motivation of this work is related to PP, the

emphasis of this current communication will be shown to concentrate on gas phase reactions and -energetics.

The PP literature has long been interested in correlating deposition kinetics, physico-chemical and structural properties of films with energy absorbed by the organic precursor (or *monomer*) molecules in the plasma. In work of Hegemann and coworkers [49-51], who developed an original approach towards the macroscopic phenomenology of PP, the parameter W/F (W being power input, and F the monomer flow rate) is proportional to the average energy transferred per monomer molecule during its travel through the active plasma zone, and it governs the formation of reactive intermediates. It was originally known as the Becker parameter [52], or since the late 1970s as the Yasuda parameter [39, 53], W/FM (energy per mass of monomer), M being molecular mass of the monomer. Depending on its relative magnitude, W/F allows one to identify different operating regimes, so-called *monomer-lean* (excess energy, later referred to as *region I*), or *monomer-rich* (energy-deficient, later *region II*) in the PP process, usually leading to films with very different structures and characteristics. Accurate knowledge of energy-uptake per molecule should, in principle, facilitate plasma process design well before the point of examining ensuing coating properties. This, in turn, should enable (i) predicting outcomes when using new molecular precursors; (ii) comparison of data from different laboratories; and (iii) reactor scale-up for industrial implementation.

Now, all of the work regarding energy measurements mentioned so far pertained to plasmas under partial vacuum, where the reagent (monomer) feed is usually undiluted, and where energy absorbed by the discharge can be evaluated relatively simply and precisely. This is *very* different in the case of AP DBD plasmas, where the discharge must be sustained in a flow of (inert) carrier gas (e.g. Ar or He) with typically a few parts per thousand (‰) concentrations of reagent or monomer (hereafter often referred to as *dopant*), and where accurate determination of energy, especially the portion absorbed by the reagent molecules, had hitherto not been possible or even attempted. The physics of energy transfer to the reagent gas molecules differs greatly between LP and AP plasmas. In the former, this occurs largely through inelastic collisions with “hot” electrons and some photo-induced bond breakage due to energetic ultraviolet (UV) photons emitted by the plasma,[11] while in the latter it results from yet a third important source, Penning-transfer during collisions with excited metastable Ar* or He* atoms; in the case of Ar, used here, the lowest energy of metastable [Ar($4s^3P_2$)] Ar* atoms is 11.55 eV. We believe that the work

reported here constitutes an innovative breakthrough in that it allows, for the first time, accurate determination of energy per reagent molecule during DBD-based plasma-chemical processing.

A.2 Experimental

Very recently, we developed and reported a methodology for measuring, E_g, the energy dissipated per cycle of the applied a.c. high voltage, $V_a(f)$, in a large-area (A = 216 cm^2) DBD reactor destined for PP research [9]. The inert carrier gas flow was F = 10 standard liters per minute (slm) of pure argon (Ar), the DBD plasma being sustained by audio-frequency ($20 \leq f \leq$ 40 kHz, usually 20 kHz) high voltage, typically $V_a(f)$ = 2.8 kV_{rms} (= 8 kV_{pp}, peak-to-peak). To our pleasant surprise, we discovered that the addition of a few ‰ of *dopant* (reagent or monomer) gas resulted in a *precisely* reproducible value of energy difference, ΔE_g, with and without *dopant* in the Ar flow, the estimated uncertainty in E_g and ΔE_g being < 5% [9]. That first report was largely devoted to describing the reactor system design, and the MATLAB®-based acquisition and treatment of DBD voltage, $V(t)$, and current, $I(t)$, data that underlie E_g measurements. A few simple examples based on diatomic or light hydrocarbon reagents were also presented, albeit rather superficially. The purpose of this letter is to illustrate how ΔE_g as a function of *dopant* flow rate, F_d, can yield subtle information in cases of dopant molecules (*monomers*) with more complex structures. The product ($\Delta E_g \times f$) divided by the number of molecules per second ($\propto F_d$) equals E_m, the characteristic energy (in eV) per molecule in the discharge. In other words, the plasma resembles a "reservoir" that provides the measured amount of energy (E_m) to the particular "molecular cocktail" that exists in the gas phase for any particular F_d value, other experimental parameters being fixed [9].

A.3 Results and Discussion

The particular case we have selected for the purpose described above is a family of three organic acids, namely formic, acetic and acrylic acid, the latter being a frequently-used monomer for PP experiments,[4, 13] and one that has been the object of controversy in the literature, particularly regarding the above-referenced macroscopic modeling [48]. Chemical formulae of the three organic acids, and their molecular masses, M, are shown in Scheme A.1:

(i) (ii) (iii)

Scheme A.1. (i) Formic acid (M = 46.0); (ii) Acetic acid (M = 60.0); (iii) Acrylic acid (M = 72.0).

Figure A.1(a), which relates to each of the three molecules presented in Scheme A.1, shows sharp rises in ΔE_g with increasing F_d, followed by near-constant plateaus; (b) shows maximum values of E_m at low F_d, followed by monotonic decreases with near $1/F_d$ behavior, as will appear presently. Key characteristics to emerge from (b) are those peak values of E_m, $(E_m)_{max}$, found to be 10.5, 59.3, and 64.0 eV for compounds (i), (ii) and (iii), respectively. These peaks clearly separate the "*monomer-lean*" (energy-rich, low F_d, *region I*) and "*monomer-rich*" (energy-deprived, high F_d, *region II*) domains. We shall return to the interpretation of $(E_m)_{max}$ values further below. The uncertainty of E_m is dictated by that of F_d, being lowest (< 5%) for larger F_d, and highest (< 15%) for the very smallest F_d; for molecules with low volatility, F_d is determined gravimetrically.

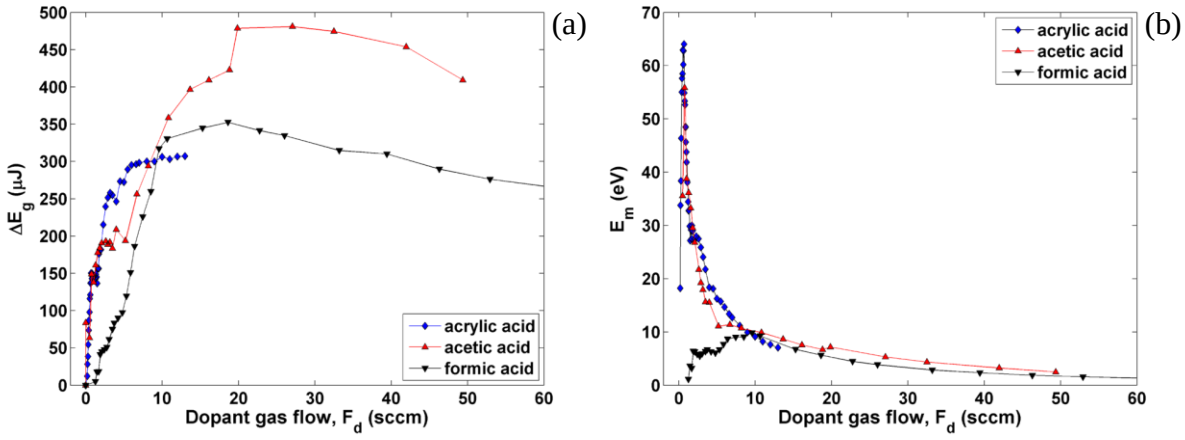

Figure A.1. (a) Plot of ΔE_g, and (b) E_m (in eV, see text) versus F_d for three organic acids shown in Scheme 1 (f = 20 kHz, V_a = 2.8 kV_{rms}, F = 10 slm).

In Figure A.2 (a), we show another plot of E_m, but this time versus $1/F_d$, which reverses regions I and II; (b) shows a zoom on the region closest to the origin (lowest $1/F_d$ values, or

highest dopant flow rates), where near-linear behavior is observed. From a simple dimensional analysis, the slope can be shown to have distinct physical meaning, namely power provided by the DBD plasma to the dopant; alternatively, it can be interpreted as the facility of the particular dopant to absorb energy from the Ar plasma's energy "reservoir". The respective values for compounds (i), (ii) and (iii) are 7.4, 6.8, and 5.6 W. Returning to Figure A.2 (a), we note that E_{m} drops to low values for high $1/F_{\mathrm{d}}$ (low F_{d}) and that positions of $(E_{\mathrm{m}})_{max}$ shift to higher $1/F_{\mathrm{d}}$ as one proceeds from (i) to (iii). Knowing that (i) and (ii) do not result in appreciable film deposition, contrary to (iii), this suggests that a "critical" threshold value of molecular mass, M, must exist between those of (ii) and (iii). Although not apparent in Figure A.2 (a), we believe that the double bond in AA also plays an important role in favoring plasma-initiated oligomerization / polymerization; PP AA is of course well documented in the literature [50, 83], as well as in our own experiments (not shown here).

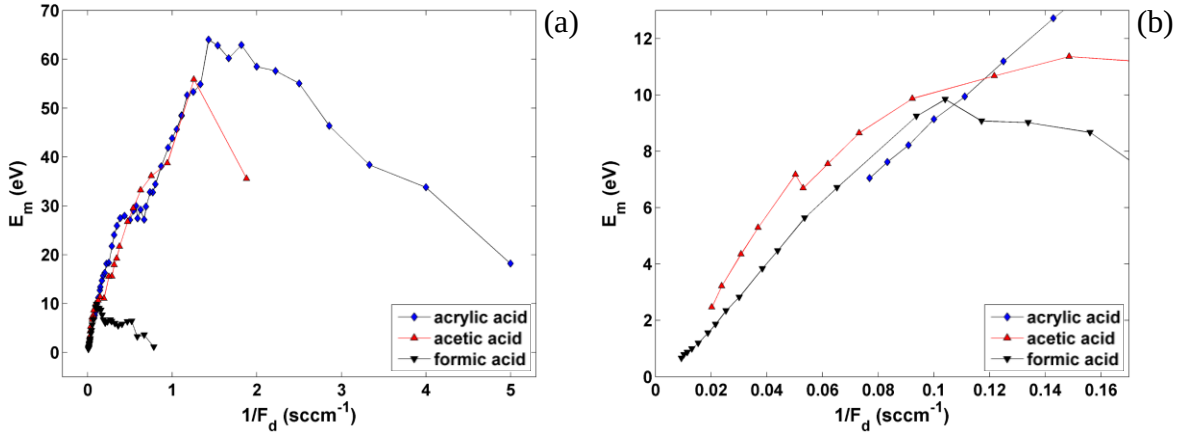

Figure A.2.(a) Plot of E_{m} (in eV) versus $1/F_{\mathrm{d}}$ for three organic acids shown in Scheme 1; (b) region closest to the origin (f = 20 kHz, V_{a} = 2.8 $\mathrm{kV_{rms}}$, F = 10 slm).

Figure A.3 shows $(E_{\mathrm{m}})_{max}$ plotted versus M for a broad range of gases and vapors, nearly all carbon-based (i.e. "organic"). One clearly notes the trend of these data, corresponding to very diverse chemistries (but in many cases families of compounds), to fall into a broad pie-shaped band extending from the lower left towards the upper right of the plot. In reference [9] we reported data pertaining to the lower left-hand corner (O_2, N_2, hydrocarbons) and pointed out good agreement with Hegemann's E_{a} values obtained with LP plasmas [49-51]. We have emphasized the three data points that correspond to (i), (ii) and (iii) by larger red triangles and bold labeling. The trend portrayed by Figure A.3 is entirely logical: simple (low-M) gases like H_2, O_2, N_2, CO_2

merely undergo excitation, dissociation or ionization reactions, as reflected by $(E_{\mathrm{m}})_{max} \leq 20$ eV, while large-M organic compounds display higher values of $(E_{\mathrm{m}})_{max}$. The family of esters, shown on the right-hand side of Figure A.3, deserves some special mention: Unsaturated compounds with double or triple bonds, but quite similar M values, are seen to possess larger $(E_{\mathrm{m}})_{max}$ values, possibly due to oligomerization in the gas phase; these questions are now the objects of further investigations. The families of esters and organosilicons will be the objects of separate reports elsewhere, along with correlations between E_{m} values, growth kinetics and PP film structures.

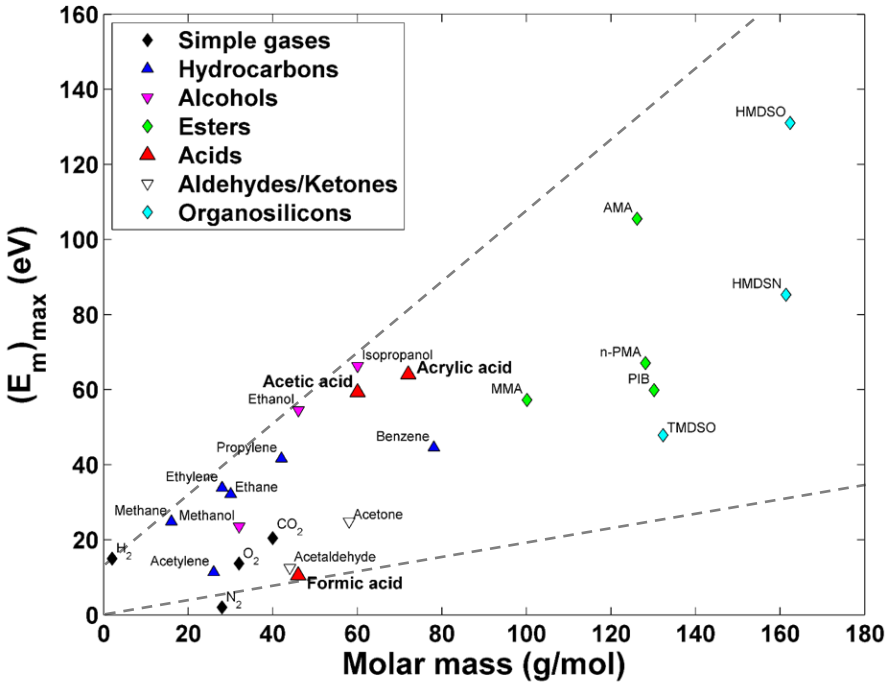

Figure A.3. Plot of $(E_{\mathrm{m}})_{max}$ (in eV) versus molecular mass, M, for a series of simple gases and more complex organic molecules. Explanation of abbreviations: MMA: methyl methacrylate; PIB: propyl isobutyrate; n-PMA: n-propyl methacrylate; AMA: allyl methacrylate; TMDSO: tetramethyldisiloxane; HMDSN: hexamethyldisilazane; HMDSO: hexamethyldisiloxane (f = 20 kHz, $V_{\mathrm{a}} = 2.8$ $\mathrm{kV_{rms}}$, F = 10 slm).

Finally, Table A.1 summarizes numerical values of slopes (power, in Watts) and of $(E_{\mathrm{m}})_{max}$ corresponding to the compounds portrayed in Figure 3, and collected according to memberships in particular chemical families. While we have just commented on the rise of $(E_{\mathrm{m}})_{max}$ with increasing M, it is striking to note near-constant slopes in the cases of certain families, such as the

alkenes, alcohols, esters and aldehydes/ketones, in the monomer-rich regions (low-energy conditions). This would confirm their very similar propensity to absorb power from the DBD Ar plasma on account of comparable plasma-chemical reaction pathways. The fact that the slope (power) values differ somewhat among the organic acids is probably attributable to different bond breakages and ensuing different reactions in each case.

Table A.1. Numerical values of slopes (in Watts) and $(E_{\mathrm{m}})_{max}$ (in eV) for all compounds presented in Figure A.3.

Family	**Molecule**	**Slope (W)**	**$(E_{\mathrm{m}})_{\mathrm{max}}$ (eV)**
Hydrocarbons	Methane	2.7	24.8
	Ethane	8.5	32.1
	Propylene	12.1	41.7
	Ethylene	12.2	33.9
	Acetylene	13.0	11.5
	Benzene	13.8	44.6
Simple gases	Nitrogen	1.6	1.9
	Hydrogen	5.9	15.0
	Oxygen	6.3	13.6
	Carbon dioxide	5.6	20.4
Alcohols	Methanol	8.3	23.5
	Ethanol	8.5	54.5
	Isopropanol	8.0	66.3
Acids	Formic Acid	7.4	10.5
	Acetic Acid	6.8	59.3
	Acrylic Acid	5.6	64.0
Esters	Methyl Methacrylate	11.5	57.3
	Propyl Isobutyrate	10.2	59.9
	n-Propyl Methacrylate	9.9	67.1
	Allyl Methacrylate	9.8	105.5
Aldehydes/Ketones	Acetaldehyde	8.9	12.5
	Acetone	9.4	24.8
Organosilicons	Hexamethyldisilazane	10.1	85.3
	Hexamethyldisiloxane	12.3	131.0
	Tetramethyldisiloxane	12.0	47.9

A.4 Outlook

Plasma polymers (PP) have achieved prominent status in various technological applications [89], especially in bio-technology [90]. Both of these references address a commercially-important example, extended-wear contact lenses: High-permeability silicone hydrogel lenses transmit sufficient oxygen so that they can be worn for up to 30 days, but Ciba Vision's "*Night & Day*" brand adds a proprietary plasma polymer coating with enhanced wettability for the wearer's comfort, and for reduced lipid-based biofilm formation. Another example from our own laboratories is PP-deposition onto electrospun nanofiber synthetic vascular grafts, where an amine-rich coating enables formation and strong adhesion of a complete endothelial lining, necessary to inhibit thrombosis [91]. The literature is replete with such examples that stress careful control of fabrication parameters, notably W/F or W/FM, but the vast majority of these involve LP plasmas, clearly not the most economical. As mentioned above, the innovative and powerful approach we have described here is expected to push forward the cheaper, easier to up-scale AP DBD plasma-coating methodology; to start, we shall investigate the families of esters and organosilicons in the right-hand portion of Figure A.3.

Acknowledgements: The authors are grateful for financial support from the Natural Sciences and Engineering Research Council of Canada (NSERC) and from the *Fonds de recherche du québec – nature et technologies* (FRQNT). we thank Dr. Hervé Gagnon for valuable assistance, and Yves Leblanc for skilled technical help.

APPENDIX B FULL LIST OF PUBLICATIONS INVOLVING THE AUTHOR'S CONTRIBUTION

[1] S. Watson, B. Nisol, S. Lerouge, and M. R. Wertheimer, *"Energetics of Molecular Excitation, Fragmentation and Polymerization in a Dielectric Barrier Discharge with Argon Carrier Gas," Langmuir*, 2015, *vol. 31, no. 37*, pp. 10125-10129.

[2] B. Nisol, S. Watson, S. Lerouge, and M. R. Wertheimer, *"Energetics of Reactions in a Dielectric Barrier Discharge with Argon Carrier Gas: II Mixtures with Different Molecules," Plasma Process. Polym.*, 2016, *vol. 13, no. 5*, pp. 557-564.

[3] B. Nisol, S. Watson, S. Lerouge, and M. R. Wertheimer, *"Energetics of Reactions in a Dielectric Barrier Discharge with Argon Carrier Gas: III Esters," Plasma Process. Polym.*, 2016, *vol. 13, no. 9*, pp. 900-907.

[4] D. Hegemann, B. Nisol, S. Watson, and M. R. Wertheimer, *"Energy Conversion Efficiency in Plasma Polymerization – A Comparison of Low- and Atmospheric-Pressure Processes," Plasma Process. Polym.*, 2016, *vol. 13, no. 8*, pp. 834-842.

[5] B. Nisol, S. Watson, S. Lerouge, and M. R. Wertheimer, *"Energetics of Reactions in a Dielectric Barrier Discharge with Argon Carrier Gas: IV Ethyl Lactate," Plasma Process. Polym.*, 2016, *vol. 13, no. 10*, pp. 965-969.

[6] D. Hegemann, B. Nisol, S. Watson, and M. R. Wertheimer, "*Energy Conversion Efficiency in Low- and Atmospheric-Pressure Plasma Polymerization Processes, Part II: HMDSO," Plasma Chem. Plasma Process.*, 2017, *vol. 37, no. 1*, pp. 257–271.

[7] B. Nisol, S. Watson, S. Lerouge, and M. R. Wertheimer, *"Energetics of Reactions in a Dielectric Barrier Discharge with Argon Carrier Gas: V Hydrocarbons," Plasma Process. Polym.*, 2017, *vol. 14, no. 8*, e. 1600191.

[8] B. Nisol, S. Watson, A. Meunier, D. Juncker, S. Lerouge, and M. R. Wertheimer, *"Energetics of reactions in a dielectric barrier discharge with argon carrier gas: VI PEG-like coatings," Plasma Process. Polym.*, 2018, *vol. 15, no. 3*, e. 1700132.

[9] B. Nisol, S. Watson, Y. Leblanc, S. Moradinejad, M. R. Wertheimer, and A. Zamyadi, *"Cold plasma oxidation of harmful algae and associated metabolite BMAA toxin in aqueous suspension," Plasma Process. Polym.*, 2019, *vol. 16, no. 2*, e. 1800137.

[10] J. Mertens, S. Watson, B. Nisol, M. R. Wertheimer, and F. Reniers, *"Energetics of reactions in a dielectric barrier discharge with argon carrier gas: VII anhydrides," Plasma Process. Polym.*, 2019, *vol. 16, no. 5*, e. 1800186.

[11] D. Hegemann, B. Nisol, S. Gaiser, S. Watson, and M. R. Wertheimer, *"Energy conversion efficiency in low- and atmospheric-pressure plasma polymerization processes with hydrocarbons," Phys. Chem. Chem. Phys.*, 2019, *vol. 21, no. 17*, pp. 8698-8708.

[12] S. Watson, B. Nisol, H. Gagnon, M. Archambault-Caron, F. Sirois, and M. R. Wertheimer, *"Energetics of Noble Gas Dielectric Barrier Discharges: Novel Results Related to Electrode Areas and Dielectric Materials," IEEE Trans. Plasma Sci.*, 2019, vol. *47, no. 5*, pp. 2680-2688.

[13] S. Watson, B. Nisol, and M. R. Wertheimer, *"Energetics of Reactions in a Dielectric Barrier Discharge with Argon Carrier Gas: VIII Hydrofluoromethanes,", Plasma Process. Polym.*, 2019, *early view*, e. 1900125.